ANKARA YILDIRIM BEYAZIT UNIVERSITY

GRADUATE SCHOOL OF NATURAL AND APPLIED SCIENCES



SYNTHESIS OF TUNGSTEN CARBIDE AND PLATINUM COMPOSITE THIN FILMS FOR HYDROGEN PRODUCTION BY ELECTROCHEMICAL WATER SPLITTING

M.Sc. Thesis by

Ali SEMERCİ

Department of Energy Systems Engineering

June, 2018

ANKARA

SYNTHESIS OF TUNGSTEN CARBIDE AND PLATINUM COMPOSITE THIN FILMS FOR HYDROGEN PRODUCTION BY ELECTROCHEMICAL WATER SPLITTING

A Thesis Submitted to

The Graduate School of Natural and Applied Sciences of

Ankara Yıldırım Beyazıt University

In Partial Fulfillment of the Requirements for the Degree of Master of Science in Energy Systems Engineering

by

Ali SEMERCİ

June, 2018

ANKARA

M.Sc. THESIS EXAMINATION RESULT FORM

We have read the thesis entitled **" SYNTHESIS OF TUNGSTEN CARBIDE AND PLATINUM COMPOSITE THIN FILMS FOR HYDROGEN PRODUCTION BY ELECTROCHEMICAL WATER SPLITTING"** completed by **Ali SEMERCİ** under the supervisions of **Prof. Dr. Abdullah YILDIZ** and **Assist. Prof. Dr. Saim EMİN**, and we certify that in our opinion it is fully adequate, in scope and in quality, as a thesis for the degree of Master of Science.

Prof. Dr. Abdullah YILDIZ

Supervisor

Assist. Prof. Dr. Saim EMİN

Co-supervisor

Prof. Dr. Hasan OKUYUCU

Jury Member

Prof. Dr. Sefer Bora LİŞESİVDİN

Jury Member

Assist.Prof. Dr. Kouroush SALİMİ

Jury Member

Prof. Dr. Fatih V. ÇELEBİ

Director

Graduate School of Natural and Applied Sciences

ETHICAL DECLERATION

I hereby declare that, in this thesis which has been prepared in accordance with the Thesis Writing Manual of Graduate School of Natural and Applied Sciences,

- All data, information and documents are obtained in the framework of academic and ethical rules,
- All information, documents and assessments are presented in accordance with scientific ethics and morals,
- All the materials that have been utilized are fully cited and referenced,
- No change has been made on the utilized materials,
- All the works presented are original,

and in any contrary case of above statements, I accept to renounce all my legal rights.

June, 2018 Ali SEMERCİ

ACKNOWLEDGEMENT

I would like to thank my supervisor, Prof. Abdullah YILDIZ, and my co-supervisor Asist. Prof. Saim EMİN for their guidance, encouragement, and advice. I would also like to thank the members of staff at Ankara Yıldırım Beyazıt University and University of Nova Gorica for the support during study and research work.

Completing this work has been the support and friendship provided by my colleague Cesur ALTINKAYA who is research assistant.

I must express my gratitude to my mother Sevdiye SEMERCİ, and my fiancee Nurgül AKPINAR for their continued support and encouragement.

Finally, I would like to thank the members of Materals Research Laboratory at the University of Nova Gorica, Slovenia, for providing me me help and allowing me access to excellent research facility to undertake this research. I thank also the Erasmus+ mobility program of EU for providing me financial support during my stay at the University of Nova Gorica.

SYNTHESIS OF TUNGSTEN CARBIDE AND PLATINUM COMPOSITE THIN FILMS FOR HYDROGEN PRODUCTION BY ELECTROCHEMICAL WATER SPLITTING

ABSTRACT

In this study, tungsten carbide and platinum composite electrocatalyst materials performances in Hydrogen evolution reaction (HER) were explored. The preparation of tungsten carbide catalysts was performed by spin-coating of colloidal tungsten (W) nanoparticles (NPs) onto graphite (C) substrates. Tungsten carbide phases (W_2C and WC) were produced applying heat treatment to W/C samples at elevated temperatures under inert atmosphere. To characterize different phases combination of methods were used such X-Ray Diffraction (XRD), Scanning Electron Microscopy (SEM), Transmission Electron Microscopy (TEM), Differential Scanning Calorimetry (DSC), X-Ray Photoelectron Spectroscopy (XPS) measurements were performed. To evaluate the electrochemical properties of different catalyst materials Linear Sweep Voltammetry (LSV), Elecktrochemical Impedance Spectroscopy (EIS) were used. The thesis demonstrates a novel way for preparation of metal carbides using combination of methods such as wet-chemistry and combustion synthesis techniques. The present synthetic approach allows preparation of active HER electrocatalysts based on tungsten carbides.

Keywords: Tungsten carbide, hydrogen evolution, overpotential, electro-catalayst, platinum composite

ELEKTROKİMYASAL SU AYIRMA YÖNTEMİ İLE HİDROJEN ÜRETİMİ İÇİN TUNGSTEN KARBÜR VE PLATİN KOMPOZİT İNCE FİLMLERİN SENTEZİ

ÖZ

Bu çalışmada, tungsten karbit ve platin komposit elektrokatalizör malzemelerin Hidrojen Oluşum Reaksiyonu (HER) performansları incelenmiştir. Tungsten karbür katalizörlerin hazırlanması, grafit alt katmanlar (C) üzerine kollodial tungsten (W) nano parçacıkların spin-coating yolu ile gerçekleştirildi. İnert atmosfer altında yüksek sıcaklıklarda W/C numunelerine ısıl işlem yoluyla tungsten karbür fazları (W_2C and WC) üretildi. Farklı fazları karakterize etmek için X-Işını Kırınımı (XRD), Taramalı Elektron Mikrosposi (SEM), Geçirimli Elektron Mikroskopisi (TEM), Diferansiyel Taramalı Kalorimetre (DSC), X-Işınları Fotoelektron Spektroskopi (XPS) ölçümleri gerçekleştirildi. Farklı katalizör malzemelerin elektrokimyasal özelliklerini değerlendirmek için, Lineer Süpürme Voltametri (LSV), Elektrokimyasal İmpedans Spektroskopi (EIS), Tafel eğimi ölçümleri kullanıldı. Tez, ıslak kimya ve yanma sentez teknikleri gibi metodların kombinasyonunu kullanarak metal karbürlerin hazırlanması için yeni bir yol göstermektedir. Mevcut sentetik yaklaşım, tungsten karbürlere dayanan aktif HER elektrokatalizörlerinin hazırlanmasına olanak tanımaktadır.

Anahtar Kelimeler: Tungsten karbür, hidrojen oluşum, aşırı potensiyel, elektro katalizör, platin kompozit,

CONTENTS

M.Sc. THESIS EXAMINATION RESULT FORM ii
ETHICAL DECLERATION iii
ACKNOWLEDGEMENT iv
ABSTRACT v
ÖZ vi
ABBREVIATIONS ix
LIST OF SYMBOLS xii
LIST OF TABLES xiv
LIST OF FIGURES xv

CHAPTER 1 - INTRODUCTION 1
1.1 Histrocial Information on Water Electrolysis 3
1.2 The Chemistry of Water Splitting by Electrolysis 4
1.3 The Aim of Thesis 6

CHAPTER 2 - HYDROGEN EVOLUTION REACTION 7
2.1 Overpotential 10
2.2 Onset Potential 11
2.3 Exchange Current Denstiy 11
2.3 Tafel Slope 12
2.4 Gibbs Free Energy 14
2.5 Electrocatalysis 15
2.6 Earth-Abundant Electrocatalysis for HER 16
2.7 Literature Review 19

CHAPTER 3 - EXPERIMENTAL STUDIES 21
3.1 Synthesis of Electrocatalyst Materials 21
3.1.1 Synthesis of Platinum (Pt) NPs 21
3.1.2 Synthesis of Tungsten (W) NPs 21
3.1.3 Synthesis of 5%Pt-W NPs 22
3.2 Preparation and Spin Coating of Electrodes 22
3.3 Heat Treatment of Electrodes 24

3.4 Material Characterization Techniques 26
3.4.1 X-Ray Diffraction (XRD) 26
3.4.2 Scanning Electron Microscopy (SEM) 27
3.4.3 Transmission Electron Microscopy (TEM) 28
3.4.4 Differential Scanning Calorimetry (DSC) 29
3.4.5 X-Ray Photoelectron Spectroscopy (XPS) 31
3.5 Electrochemical Measurement Techniques 31
3.5.1 Three-Electrode Cell 32
3.5.2 Linear Sweep Voltammetry (LSV) 33
3.5.3 Electrochemical Impedance Spectroscopy (EIS) 34

CHAPTER 4 - RESULTS AND DISCUSSION 36
4.1 Characterization Results of Pt, WC, W_2C 36
4.2 Electrochemical Measurement Results 45
4.2.1 Linear Sweep Voltammetry and Stability Test 45
4.2.2 XPS Measurement Results 52

CHAPTER 5 - CONCLUSIONS 54
REFERENCES 55

CURRICULUM VITAE 69

ABBREVIATIONS

AC	Alternating Current
Al	Aluminum
Ag/AgCl	Silver silver Chloride Electrode
Ar	Argon
C	Carbon
CE	Counter Electrode
$CHCl_3$	Chloroform
Co	Cobalt
CO	Carbon Monoxide
CO_2	Carbon dioxide
Cr	Chromium
DSC	Differential Scanning Calorimetry
EDS	Energy Dispersive Elemental
EIS	Electrochemical Impedance Spectroscopy
EtOH	Ethanol
Fe	Iron
H_2	Hydrogen
H^+	Proton
H_{ads}	Adsorbed Hydrogen Atoms
HER	Hydrogen Evolution Reaction
H_2S	Hydrogen Sulfide
H_2SO_4	Sulfuric Acid
Ir	Iridium
LSV	Linear Sweep Voltammetry
Mg	Magnesium
ml	Mililiter
Mo	Molybdenum

NHE	Normal Hydrogen Electrode
Ni	Nickel
nm	Nanometer
NPs	Nanoparticles
RE	Referance Electrode
O_2	Oxygen
ODE	Octedecene
OE	Oleic Acid
OLA	Oleyamine
OER	Oxygen Evolution Reacktion
Pd	Paladium
Ph	Power of Hydrogen
Pt	Platinum
$Pt(acac)_2$	Platinum(II) acetylacetonate
RE	Referance Electrode
RHE	Reversible Hydrogen Electrode
Ru	Ruthenium
SEM	Scannin Electron Microscopy
SHE	Standart Hydrogen Electrode
SPE	Solid Polymer Electrolyte
TEM	Transmission Electron Microscopy
TMCs	Transition Metal Carbides
W	Tungsten
WC	Tungsten Carbide
W_2C	Ditungsten Carbide
$W(CO)_6$	Hexacarbonyltungsten
WE	Working Electrode
XRD	X-Ray Diffraction
XPS	X-ray Photoelectorn Spectroscopy

μm	Micrometer

LIST OF SYMBOLS

b	Tafel Slope, $mVdec^{-1}$
E_{cell}	Electrode Potential, V
E^0	Standart Electrode Potential, V
$E^0_{cathode}$	Standard Electrode Potential of The Cathodic Half Reaction, V
E^0_{anode}	Standard Electrode Potential of The Anodic Half Reaction, V
$E_{Ag/AgCl}$	Silver Silver Chloride Electrode Potential, V
$E^o_{Ag/AgCl}$	Silver Silver Chloride Standard Electrode Potential, V
E_{NHE}	Normal Hydrogen Electrode Potential
E_{RHE}	Reversible Hydrogen Electrode Potential
E_{th}	Termoneutral Electrode Potential, V
E_w	Frequency-Dependent Potential, V
F	Faraday Constant, 9,648 $x10^4$ (C/mol)
H	Plank Constant, 3.626 10^{-34} Js^{-1}
I_w	Frequency-Dependent Current, Amper
j	Current Density, mA/cm^2
j_0	Exchange Current Density, mA/cm^2
n	Number of Moles of Electrons
Q	Reaction Quotient
R	Universal Gas Constant, 8,314 J/Kmol
R	Resistance , Ω
R_{ct}	Charge-transfer Resistance, Ω
T	Temperature, K
Z_{imag}	Imaginary Component of Impedance, Ω
Z_{real}	Real Component of Impedance, Ω
Z_{total}	Total Impedance, Ω
Z_w	İmpedance, Ω μm,
η	Overpotential, V

η_0	Onset Potential, V
η_{10}	Overpotential at j= 10 mA/cm^2
ΔG	Gibbs Free Energy, J/mol
ΔH	Enthalpy, kJ/mol
ΔG_H	Free Energy of Hydrogen Adsorption, J/mol
α	Transfer Coefficient

LIST OF TABLES

Table 4.1 Promising tungsten based carbides used in HER studies 49
Table 4.2 Tungsten supported Pt used in HER studies 50

LIST OF FIGURES

Figure 1.1 Routes for Production of Hydrogen 2

Figure 1.2 Schematic Diagram of an Electrolyzer 2

Figure 1.3 Average Production Prices of hydrogen production using different methods (per kg of H_2) 3

Figure 2.1 Pourbaix diagram water, including equilibrium zones for water, oxygen and hydrogen at standard temperature and pressure 8

Figure 2.2 Hydrogen Evolution Reaction steps 10

Figure 2.3 Hydrogen Evolution Reacktion mechanism and Tafel slope 13

Figure 2.4 Tafel Plot 14

Figure 2.5 Volcano plot showing Sabatier principle 15

Figure 2.6 Illustriation of Volcanı plot for HER for different materials 17

Figure 2.7 The comparison between the HER catalytic activities (the over-potentials at 10 mA cm^{-2}) of the VIB transition metal carbides and Pt-loaded carbides 18

Figure 3.1 The prepared graphite electrodes ..... ….23

Figure 3.2 Spin Coating Process 23

Figure 3.3 WS-400B-6NNP/LİTE Spin Coater 24

Figure 3.4 Heat treatment process 24

Figure 3.5 Protherm Heat Furnace 25

Figure 3.6 Electrodes of after heat treatments 25

Figure 3.7 Rigaku Miniflex 600 XRD 26

Figure 3.8 Bragg's Law 27

Figure 3.9 Jeol JSM 7100F-SEM 28

Figure 3.10 JEOL 2100F-TEM 29

Figure 3.11 TGA/DSC 2 Star System 29

Figure 3.12 Working Process of DSC 30

Figure 3.13 Photoelectric emission process of electrons 31

Figure 3.14 EDAQ SP1- Potentiostat 32

Figure 3.15 Three electrode configuration scheme (left) and a photo of the used cell (right) 33

Figure 3.16 Ilustration of Linear Potential Sweep in LSV [88]. 34

Figure 4.1 TEM images of synthesized Pt nanomaterials at different magnifications and diffractograms (lower right) taken from the object in shown in upper right corner 36

Figure 4.2 TEM images of synthesized W nanomaterials 37

Figure 4.3 XRD patterns of W, W_2C, WC and their mixed phases. Reference patterns of W, W2C and WC are given with labels. 38

Figure 4.4 DSC curves of W sample heat treated with a ramp 20 °C/min under N2 atmosphere 39

Figure 4.5 SEM images of (a) pure graphite and (b-e) W NPs coated graphite substrates prepared at 900°C. In (d-f) are given images with elemental maps for W taken from the object shown in (c). The image in (e) is an overlay of W map with (c). Magnified image of W 41

Figure 4.6 SEM images of W samples heat treated at (a) 1000°C, (b) 1150°C, and (f) 1450°C. In (c) is given an SEM image and elemental maps for (d) W and (e) C of W sample prepared at 1150°C. The scale bars: (a,b) 300 nm, (c-e) 2.5 ηm and (f) 1 ηm. 42

Figure 4.7 In (a), (b), SEM images of 5%Pt-W samples heat treated at 900°C. (c), (d) is elemental maps for Pt and W respectively. The scale bars: (b) 1 ηm, (a, c, d) 2,5 ηm..... 43

Figure 4.8 In (a), (b), SEM images of 5%Pt-W samples heat treated at 1150°C. (c), (d) is elemental maps for Pt and W respectively.The scale bars: (a) 10 ηm., (b, c, d) 1 ηm..... 44

Figure 4.9 (a, b) TEM image of WC nanosheet at different magnifications. The inset in (b) is an electron electron diffraction image. 45

Figure 4.10 (a) Polarisation curves of W/C films heated treated at different temperatures (one compartment cell). The linear sweep voltammograms are recorded in 0.5 M H_2SO_4 with a scan rate of 2 mV/s. The reference Pt-C electrode is prepared by coating Pt NPs on graphite. In (b) are given Tafel plots for the different electrodes. Polarisation curves of the sample heat treated at 1150°C (c) without and (d) with Nafion membrane after the 1-st and 1000-th cycles..... 47

Figure 4.11 (a) Polarisation curves of 5%Pt-W/C films heated treated at different temperatures (one compartment cell). The linear sweep voltammograms are recorded in 0.5 M H_2SO_4 with a scan rate of 20 mV/s. In (b) are given Tafel plots for the different electrodes..... 48

Figure 4.12 Nyquist plot of W1150°C in 0.5M H_2SO_4 recorded with a bias from 0.0 to 350 mV. In (b) is given the charge-transfer resistance (Rct) vs overpotential. Inset is given an electrical equivalent circuit used to fit the EIS data. 52

Figure 4.13 XPS data of W1150°C film recorded after the stability test for 1000 cycles without Nafion 117 membrane. (a) Wide spectra and (b) 4f Pt signals..... 52

CHAPTER 1

INTRODUCTION

Energy has a direct effect on countries' development. In this regard, there is an ever-increasing demand for energy. Today, most of this demand is met by fossil energy fuels such as petroleum (85%), and natural gas [1]. The limited fossil fuel reserves, however, pose an impediment for satisfying the ever-emerging requirement for energy. In addition, the use of fossil fuels brings along various environmental issues such as global warming [2]. Accordingly, an increasing effort has been made and a vast number of studies has been conducted on environment-friendly renewable energy sources to reduce the dependence on fossil fuels for energy requirement. Among renewable energy sources, Hydrogen has been regarded as the energy source of future owing to its many advantages.

As an energy resource, the advantages of H_2 involve the following [3-6]:

- It is the most basic and abundant element in the universe.
- When blended with other fuels, it provides the highest energy ratio per unit mass (higher heating value: 140.9 MJ/kg, lower heating value 120,7 MJ/kg). The energy produced by 1 kg of hydrogen corresponds to those produced by 2.1 kg of natural gas or 2.8 kg of coal.
- H_2 is 1.33 times more efficient than petroleum products.
- It is a zero-emission fuel (no CO_2), that is, only water vapor is produced upon its combustion.
- Storability of the energy obtained from other energy sources.

Hydrogen is a secondary energy source. As shown in Figure 1, H_2 can be produced by a wide variety of energy sources using several processes. According some reports, 96% of H_2 is produced using fossil fuels, and 4% is produced via electrolysis [7].

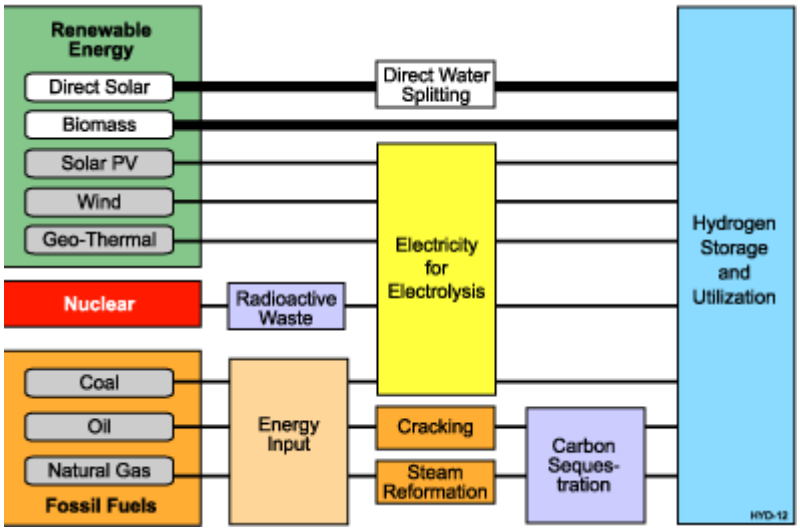


Figure 1.1 Routes for Production of Hydrogen [8].

Among the methods, shown in Figure 1.1, electrolysis is one of the most common industrial methods. Elctrolysis is the simplest and cleanest way for producing H_2. This process involves the decomposition of water into hydrogen and oxygen gases due to an electic current directly applied on water. The reaction takes place on a device called electrolyzer, which is shown in Figure 1.2.

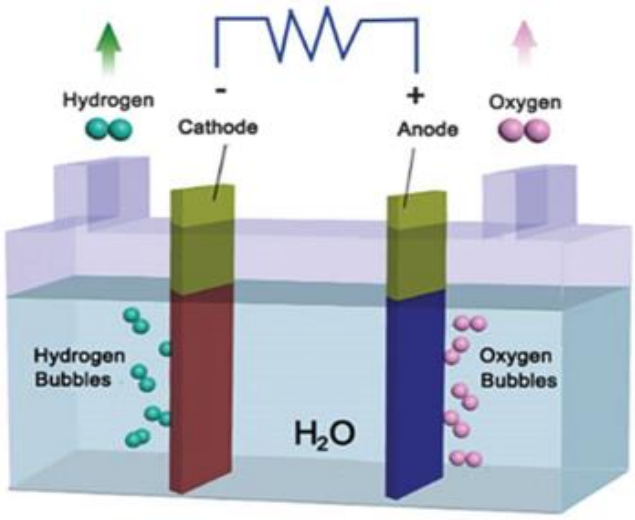


Figure 1.2 Schematic diagram of an electrolyzer [9].

H_2 production from fossil fuels is among the most commonly preferred industrial production methods, owing to its high technology and low operating costs. However,

its process simplicity in addition to the environmental concerns and acquisition of H_2 with the highest quality (>99%) renders electrolysis a more interesting subject for new studies [10]. Average production prices of different hydrogen production methods are shown in Figure 1.3.

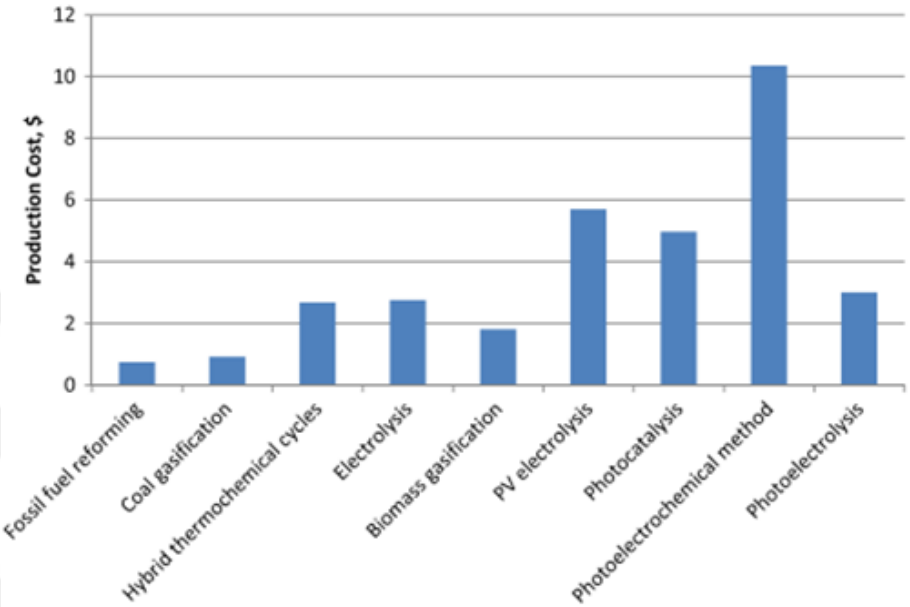


Figure 1.3 Average Production Prices of hydrogen production using different methods (per kg of H_2) [1].

1.1 Histrocial Information on Water Electrolysis

The history of water electrolysis method dates back to 1789, when Deiman and Troostwijk initially split water into hydrogen and oxygen using a Leyden Jar, device for storing static electricity [11]. They obtained H_2 with high purity (>99%) using this method [12]. In the early 1900s, H_2 production using water electrolysis method has reached an industrial scale along with the increasing H_2 demand for ammonia synthesis. In that period, water electrolysis was the most ideal method for acquisition of hydrogen with high purity. The first large scale (10000 Nm^3 H_2/h) facility for water electrolysis was established in 1939. In 1948, the first pressurized industrial electrolyzer was produced by Zdansky/ Lonza. In 1960, the first solid polymer electrolyte (SPE) was developed by General Electric company. In 1978 the first

alkaline systems applications were performed [13]. The development of water electrolysis method still continues in the present date.

1.2 The Chemistry of Water Splitting by Electrolysis

In electrolysis method, electrical current is directly applied on water. The applied electric current flows between two electrodes, which are submerged in an aqueous electrolyte with increased ionic conductivity, facilitate the flow of electric charges. By the applied current, water molecules are split into H_2 and O_2 as per equations 1.1, 1.2, 1.3 [14].

$$\text{Total reaction: } H_2O_{(l)} \longrightarrow H_{2(g)} + \frac{1}{2}O_{2(g)} \qquad E^0 = 1.23\ V \qquad (1.1)$$

$$\text{Cathode reaction: } 2H^+ + 2e^- \longrightarrow H_{2(g)} \qquad E^0 = 0\ V \qquad (1.2)$$

$$\text{Anode reaction: } \frac{1}{2}O_{2(g)} + 2H^+ + 2e^- \longleftarrow H_2O_{(l)} \qquad E^0 = 1.23\ V \qquad (1.3)$$

The electrodes are polarized when an external current is applied, one taking positive (+), and the other taking negative (-) charge. The positively charged (+) electrode is called anode and the negatively charged (-) electrode is called cathode. Water splitting occurs with two half reactions one occurring in anode electrode, and the other occurring in cathode electrode. As a result of direct application of an external current, water oxidation reaction, also referred to as oxygen evolution reaction (OER) takes place at the anode electrode. On cathode electrode side, water reduction reaction, also known as hydrogen evolution reaction (HER) occurs. O_2 and H_2 molecules, produced by these half reactions, gather at anode and cathode electrodes respectively. These half reactions occur as per equations 1.4 and 1.5 at different environments in which water splitting occurs.

In acidic solution:

$$\text{Cathode: } 2H^+ + 2e^- \longrightarrow H_{2(g)} \qquad (1.4)$$

$$\text{Anode: } H_2O \longrightarrow \frac{1}{2}O_{2(g)} + 2H^+ + 2e^- \qquad (1.5)$$

In alkaline or neutral solution:

Cathode: $2H_2O^+ + 2e^- \longrightarrow H_2 + 2OH^-$ (1.6)

Anode: $2OH^- \longrightarrow H_2O + \frac{1}{2}O_2 + 2H^+ + 2e^-$ (1.7)

The minimum voltage required for electrolysis to occur under standard conditions is represented by E_{cell} or reversible cell voltage (E_{rev}), and it can be defined by the following expression [15-16]:

$$E^0_{cell} = \frac{\Delta G^\circ}{n.F} \quad (1.8)$$

Thermoneutral cell voltage is obtained by replacing ΔG value with ΔH in equation 1.7. [17].

$$E_{th} = \frac{\Delta H^\circ}{n.F} \quad (1.9)$$

where ΔG° is the Gibbs free energy change under standard pressure and temperature, and n the number of electron (e^-) moles (n=2) transferred for each H_2 molecule. F denotes the Faraday constant (96485 C/mol). At standard pressure and temperature conditions ΔG°=237.21 kJ/mol, ΔH°=285.84 kJ/mol. The minimum energy required for water splitting can be found by plugging these values into equation 1.8, as E^0_{cell} =1.23V. However, this situation differs in practice. In real systems, this voltage is 1.48V and is defined as termoneutral electrode potential (E_{th}). The process occurs as an adiabatic process with this potential value [17-20]. E^0_{cell} value corresponds to the required theoretical voltage between cathode and anode under standard conditions, independently of the water splitting media. In other words, it is the theoretical voltage value for HER and OER [21].

$$E^0_{cell} = E^0_{cathode} - E^0_{anode} \quad (1.10)$$

1.3 The Aim of Thesis

- Synthesis of tungsten (W) nanoparticles using a facile method. As a transition metal, W and its carbides are used as electrocatalysts for HER.
- Investigation of the effect of temperature on structural change and electrocatalyst performance through application of heat treatment on tungsten thin films at different temperatures.
- Preparation of tungsten carbide (WC, W_2C) from metallic tungsten nanoparticles through heat treatment at elevated temperatures.
- The carbon required for tungsten carbide was obtained from the graphite electrodes used as substrates which is an important and original aspects of this study.
- The contribution of Tungsten, WC and W_2C to HER performance was investigated.
- Reduction of the overpotential value via acquisition of Pt doped tungsten carbide was targeted for improving HER performance.
- Contribution through introducing a new, simple and alternative way for electrocatalyst production.

CHAPTER 2

HYDROGEN EVOLUTION REACTION

HER is the cathodic half-cell reaction that occurs during Electrochemical Water Electrolysis. The general equation for HER is given in equation 2.1.

Cathode: $2H^+ + 2e^- \rightarrow H_2$ (2.1)

The mechanism of HER reactions varies depending on the pH value. Accordingly, pH is an important parameter for determination of HER rate, which takes place in both acid and alkaline media [22]. The E_{cell} value, to be applied depending on the pH value, is calculated by Nerst equation shown in equation 2.2. Nerst equation is used to calculate the thermodynamic equilibrium reduction potential at which cathodic half-cell (25°C and 1 atm) reactions occur under standard conditions or equilibrium state [23-24].

$$E_{cell} = E^0_{cell} - \frac{RT}{nF} lnQ \quad (2.2)$$

E_{cell} is the standard voltage value calculated at the applied temperature, *R* is the universal gas constant (8,314 J/Kmol), *F* is Faraday Constant (9.648 x10^4 C/mol), *n* is the number of electron moles transferred at HER, and *Q* is the reaction coefficient. For simplification of Nernst equation, *RT/F* is assumed constant at room temperature (25°C) as 0.05916 in the equation 2.3 and defined as a logarithmic expression [23, 25].

$$E_{cell} = E^0_{cell} - \frac{0{,}05916}{n} log_{10} \frac{a_{Red}}{a_{Ox}} \quad (2.3)$$

As shown in Figure 2.1, when the Nernst potential value is based on Normal Hydrogen Electrode (Standard Hydrogen Electrode) (NHE or SHE), Nernst potential value is reduced by 59 mV per increase in one unit of pH.

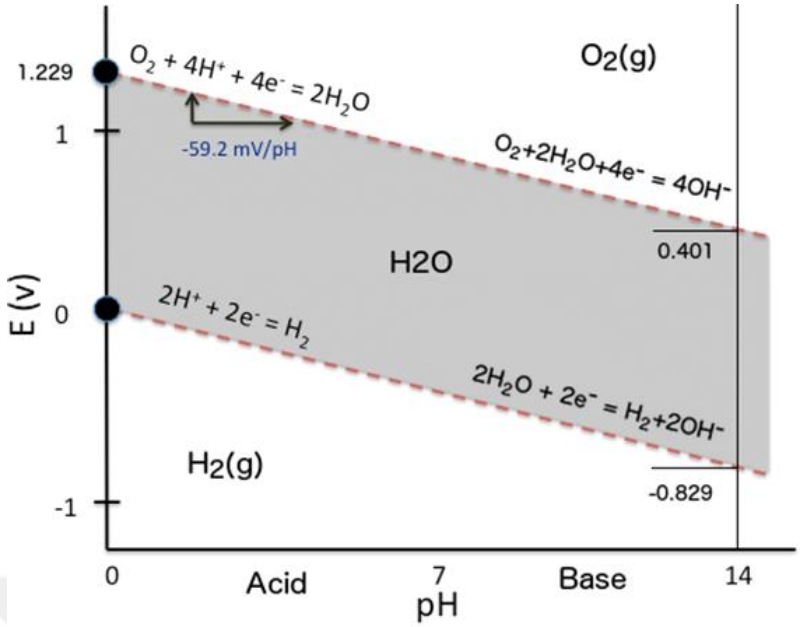


Figure 2.1 Pourbaix diagram water, including equilibrium zones for water, oxygen and hydrogen at standard temperature and pressure [26].

HER reactions are directly affected by the change in pH, accordingly the fact that the recorded potential value is not affected by the change in pH is explained through comparison with the potential value obtained using Reversible Hydrogen Electrode (RHE) which is another form of the NHE electrode. This way, the comparison of the position of the redox reaction corresponding to hydrogen's reduction potential is enabled independently from the pH value (which is always 0V vs RHE). The potential value is calculated by use of equation 2.4 obtained via conversion of Nernst equation, as per RHE [27-28].

$$E_{RHE} = E_{NHE} + 0.059 \times pH \tag{2.4}$$

In this research, Silver-silver chloride electrode (Ag/AgCl) is used as the reference electrode, in place of NHE. The measured potential value vs. Ag/AgCl value is converted to RHE value using equation 2.5.

$$E_{RHE} = E_{Ag/AgCl} + 0.059*pH + E^{o}_{Ag/AgCl} \tag{2.5}$$

In this equation, $E_{Ag/AgCl}$ denotes the potential value experimentally measured against Ag/AgCl reference electrode, and $E^{o}_{Ag/AgCl}$ denotes the standard potential value of Ag/AgCl electrode at 25°C [29].

In acidic media, HER consists of a 3-stage chain reaction [30]:

1. Volmer reaction: Hydrogen atoms are adsorbed through reduction of e^- incident from the electrode and a proton [31]

   $$H^+ + e^- \longrightarrow H_{ads} \quad (2.6)$$

2. Heyrovsky reaction: an electron and a proton combines with an adsorbed hydrogen to produce molecular hydrogen (H_2) [31].

   $$H_{ads} + H^+ + e^- \longrightarrow H_2 \quad (2.7)$$

3. Tafel reaction: H atoms adsorbed on the electrode surface are combined to produce molecular hydrogen (H_2) [31].

   $$2H_{ads} \longrightarrow H_2 \quad (2.8)$$

H_{ads} represents the hydrogen atoms adsorbed on the electrode surface. HER can follow two different possible chain reactions: Volmer-Heyrovsky or Volmer-Tafel. Both reaction mechanisms are initiated with Volmer reaction in which H atoms are adsorbed. These two different chain reactions vary depending on the electronic characteristics of the catalyzer used in HER process [32]. The Volmer, Tafel, Heyrovsky reactions constitute the most fundamental and important reactions of HER that occur on the electrode surface. However, several other parameters are available for defining HER in a better way, including Tafel slope and exchange current density. Hydrogen evolution reaction steps are shown in Figure 2.2.

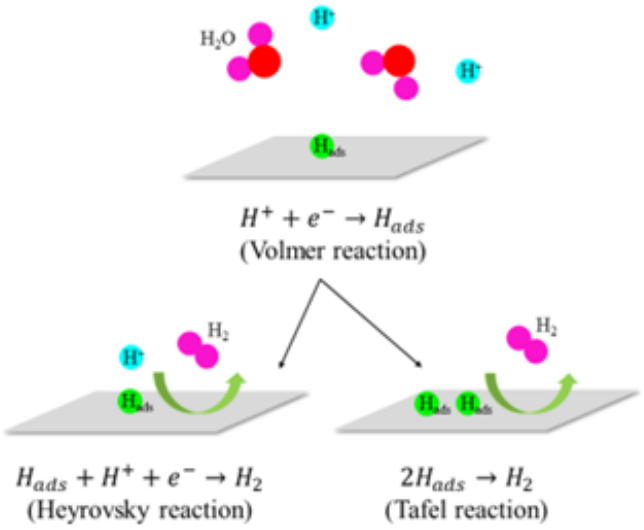


Figure 2.2 Hydrogen evolution reaction steps [32].

2.1 Overpotential

The voltage required for water splitting reactions is higher under real operating conditions. This excessive voltage value is termed as overpotential (η). Overpotential value is the difference between the applied and theoretical values. In other words, this is the amount of energy required for surpassing the reaction resistances that occur in HER for water electrolysis reactions to occur. Overpotential value is defined by equation 2.9 [33-34].

$$\eta = E_{cell} - E^0_{cell} \tag{2.9}$$

This is due to the requirement for surpassing the internal activation barrier values comprising of anode (η_a), cathode (η_c) and other resistances (solution resistance, contact resistance etc.). Applied (operational) voltage value is shown in equation 2.10 [adapted from 35]:

$$E_{cell} = 1.23V + \eta_a + \eta_c + \eta_{other} \tag{2.10}$$

As indicated in Equation 2.10, overpotential value should be reduced for a minimum voltage value and to increase HER performance. The value of overpotential, on the other hand, varies depending on the reaction kinetics that occur during the reaction.

Electron transfer is among the parameters that affect the mass transfer rate η taking place in the system at the electrolyte. Limited electron transfer rates or slower reaction substance and product transfer rates results in increased η values. Accordingly, mass transfer rate has a significant effect on HER. Although a high mass transport rate between the electrode and electrolyte is indicative of high reaction rates, this does not necessarily mean that the hydrogen production is high. High reaction rates result in production of gas bubbles at higher rates. This situation hinders the contact between the electrode and the electrolyte. The bubbles that form on cathode and anode electrode surfaces have adverse effect on the electron transfer rate between the electrode and electrolyte. This results in increased ohmic losses in the system. Overpotential is the most important parameter that acts as an indicator of electrode and electrolyte performance in water splitting half reactions [36-37].

Due to the mentioned reasons, both values are kept at the minimum possible level in practice. η_a, η_c values can be reduced via correct electrode selection for HER and OER. The industrial costs can be reduced this way. For this purpose, catalyzers with high activity are used for HER reactions to make water splitting process more efficient. Catalyzers reduce η, thereby reducing the energy barrier that needs to be exceeded for water splitting reactions to occur. In addition, the use of electrodes with wider active regions contributes to the reduction of overpotential value [38-40].

2.2 Onset Potential

There are numerous definitions for onset potential (η_0). In the simplest way it can be defined as the potential when catalytic current is initially obtained during HER [41].

2.3 Exchange Current Denstiy

Another important parameter for HER is the exchange current density (j_0). Exchange current density indicates the current density value obtained at the thermodynamic equilibrium state of oxidation and reduction reactions. j_0 is related with the reaction rate. It shows the current density value at which the electrochemical reaction in the system has the same backward and backward rate [42]. Exchange Current density value is an important parameter for performance comparison among the

electrocatalysis materials used in HER. As also mentioned in the previous section, the exchange current density value can be obtained using Tafel slope when the overpotential value equals to zero. High exchange current density values are desired for electrolysis in HER for the reaction mechanism, as this is regarded as an indication of a high catalytic activity. This also allows a more stable potential change against external effects in a more stable reaction mechanism [38, 43].

2.3 Tafel Slope

Tafel slope is one of the most important parameters for evaluating the system's kinetic parameters and the performance of materials used as electrocatalyst under operating conditions. Determination of rate determining step in an electrochemical reaction is important for evaluation of the catalyzer material performance. This value is a structural characteristic of materials used as electrode. Any reaction step of HER can be the rate determining step. If the rate determining step is Volmer reaction, angular and indented electrodes facilitate the electron transfer as these have more active regions on their surface for hydrogen adsorption. If the rate determining step is Tafel or Heyrovsky reaction, the electrode's characteristics such as surface roughness prevent gas bubble formation, thereby resulting an increase in the reaction rate. Rate determining step varies depending on the overpotential value. For instance, electron transfer rate is not as high as that of hydrogen desorption at a low potential value. In this case, the rate determining step is Volmer reaction. However, when the overpotential value is adequate for the system, Tafel or Heyrovsky reactions are also determined as the rate determining step depending on the reaction path [44].

Rate determining step can be determined using the data obtained from Tafel plot. Tafel plot is defined for overpotential as shown in equation 2.11. The equation involves 2 Tafel variables. In equation 2.11 the variable represented by j_0 (mA/cm^2) is the exchange current density, and b ($mVdec^{-1}$) represents the Tafel slope. This equation shows that a lower overpotential value is obtained against *a* low *b* value for a specified current. As shown in Figure 2.3, *b* value is defined for the region in which Tafel line shows a linear characteristic. In addition, Tafel slope can be determined using the rate determining step as well. The rate determining values of Pt determined

for HER in acidic media are; Tafel reaction at 30 mV of *b*, Volmer reaction at 120 mV, and Heyrovsky reaction at 40 mV. The catalyzer materials used in HER reactions are expected to have low Tafel slope values, which is indication of a good electrocatalyst material. Low Tafel slope values result in lower increasing rates depending on the current density in the system, thereby reducing the losses likely to occur in the system [38, 45, 46].

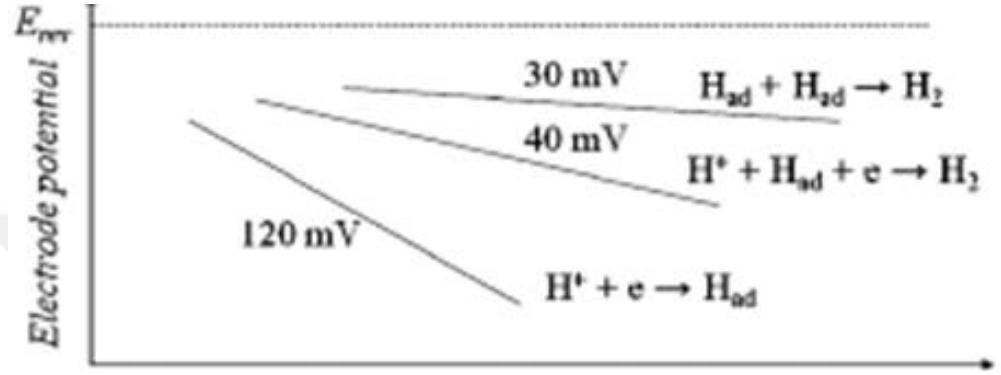


Figure 2.3 Hydrogen evolution reaction mechanism and Tafel slope [34].

As shown in equation 2.11, the correlation between overpotential and logarithmic current density is defined with Tafel slope b and exchange current density. Both data can be used for comparison of the kinetic performances of materials used as electrode at HER [37]. A value in equation 2.12 represents the Tafel interception:

$$\eta = a + b\log(j_0) \tag{2.11}$$

$$a = \frac{2.303RT}{\alpha nF}\log(j_0) \quad , \quad b = \frac{2.303RT}{\alpha nF} \tag{2.12}$$

As shown in Figure 2.4, Tafel line consists of two arms. One is the anodic arm with positive slope, and the other is the cathodic arm with negative slope. As the overpotential (η) converges to zero, Tafel line deviates from its linear behavior as shown in Figure 2.4.

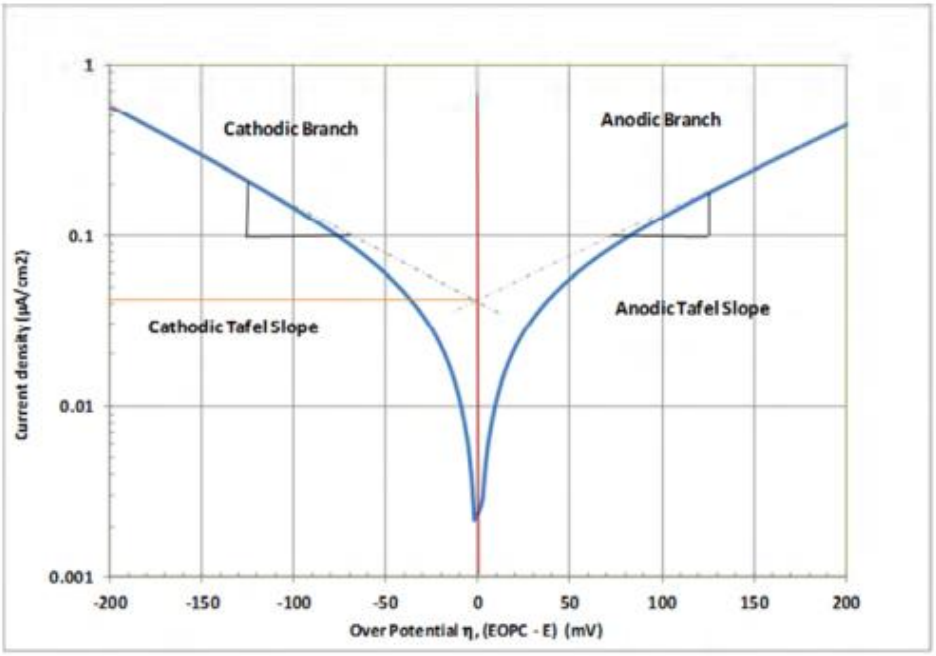


Figure 2.4 Tafel Plot [47].

If the intersection point of Tafel lines has zero overpotential, exchange current density value can be obtained from Tafel plot. This value, however, may not always yield an accurate estimation. There are some assumptions for this situation. Tafel slope is assumed to be independent of the overpotential value and it is also assumed to be constant [34].

2.4 Gibbs Free Energy

Gibbs Free Energy of Hydrogen adsorption (ΔG_H) is one of the important parameters for determination of the activity of electrocatalysis materials used in HER [48]. An ideal performance in HER mechanism is obtained with a ΔG_H value close to zero ($\Delta G_H \approx 0$). This value should not be too high or too low. When the ΔG_H value is high and positive ($\Delta G_H > 0$, endothermic), the adsorbed hydrogen atoms are adsorbed on the electrode surface with a strong bond. These situation facilities the Volmer step, and obstructs Tafel or Heyrovsky step. When the ΔG_H value is high and negative ($\Delta G_H < 0$, exothermic), a weak bond forms between the hydrogen atoms and electrode surface. Therefore, the occurrence of Volmer step, i.e. initiation of the

reaction mechanism, is hindered [9, 49-50]. By the simplest definition, when the bond between the electrode and H atoms is too strong, removal of the products from the surface is hindered, and when it is too weak, the adsorption of hydrogen is hindered. This approach is based on the Sabatier's principle [51]. The comparison of the activities of materials used as Electrocatalysis in HER is shown in Figure 2.5 The volcano plot ($log(j_0)$ vs. ΔG_H), in which the electrolysis activities in HER are compared, is formed on the basis of this principle.

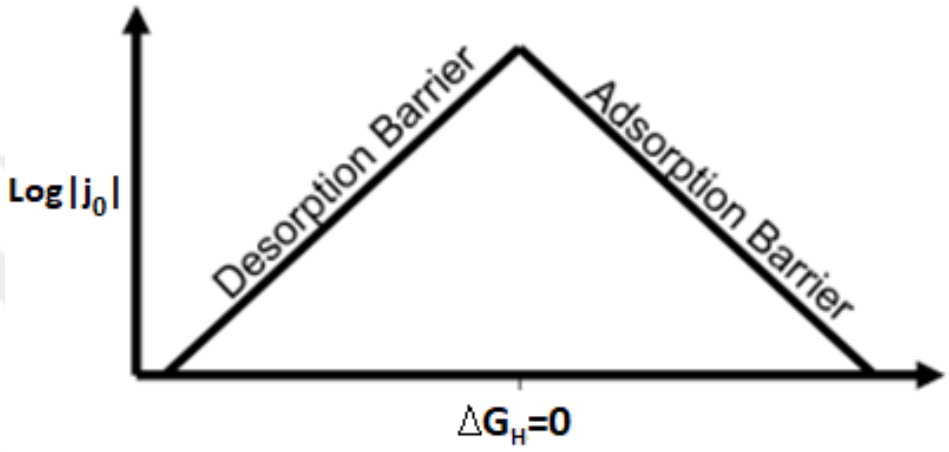


Figure 2.5 Volcano plot showing Sabatier principle [Adapten from 52].

2.5 Electrocatalysis

In the simplest term, the catalysts included in an electrochemical reaction are referred to as Electrocatalyst. The role of catalyst material in the chemical reaction is to increase the reaction rate without being affected. After the reaction a change may occur in the physical structure of the catalyst material. However, no change is observed in its chemical structure. If the reactants and the catalyst are in the same phase, these type ofcatalysts are called homogeneous catalysts, otherwise, they are called as heterogeneous catalysts. In this reaction mechanism, the molecules that emerge as reaction products are adsorbed onto the catalyst surface and the reaction takes place on the catalyst surface.

Therefore, electrocatalysts, in general, are supposed to have wide surface areas, which increases the reaction rate. In electochemical reactions, the role of catalysts is

undertaken by electrodes and electrochemical reactions occur on electrode surface. Under a constant overpotential, an electrode with higher reaction rate on its surface can be assumed to be more catalytic than another electrode with lower reaction rate on its surface [53]. The function of an electrocatalyst in the reaction mechanism is to increase the current density at a constant overpotential or to reduce the overpotential at a constant current density [54]. A well-performing electrocatalyst is supposed to have the followig characteristics [55]:

- Having a low overpotential for the reaction that will occur,
- High active surface area,
- High electrical conductivity,
- A good mechanical and chemical stability,
- Availability and low cost.

2.6 Earth-Abundant Electrocatalysis for HER

Volcano plot, shown in Figure 2.6, can be used to compare the catalytic activities of materials used as catalyst at HER. As shown in the figure, the materials with the best catalytic activity for HER mechanism are the Pt group metals (noble metals) (Platinum(Pt), Paladium (Pd), Iridium(Ir), Ruthenium(Ru), etc.). The high catalytic performance of these metals is mainly attributable to their high exchange current density and near-zero ΔG_H value. In the literature, the material with the best catalytic activity for HER mechanism is reported as Pt (j_0 = 4.5x10^{-4} A/cm^2, Tafel slope =30 mV/dec) as also shown in the Volcano plot. The near-zero overpotential value of Pt is the underlying reason for its being the electrocatalyst material [56].

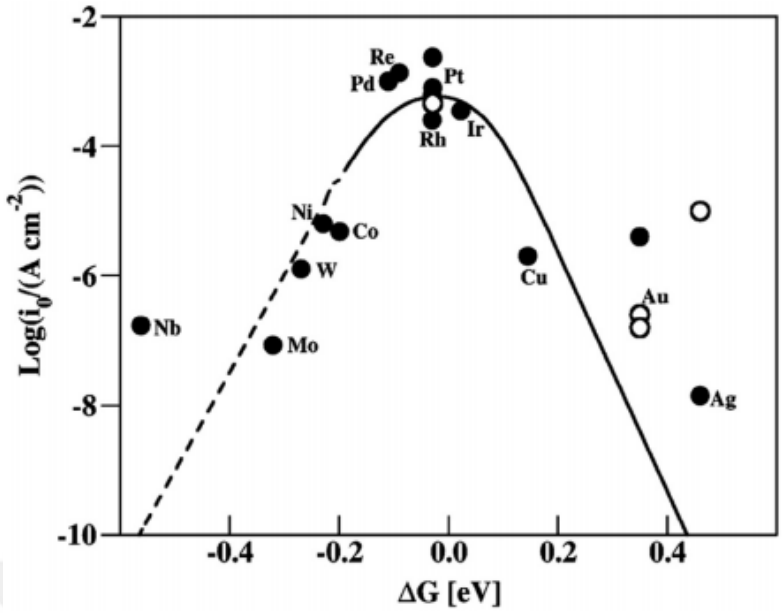


Figure 2.6 Illustriation of Volcanı plot for HER for different materials [57].

However, the scarcity of the abovementioned noble metals in the earth crust in addition to their high costs posses a serious problem for development and industrialization of the HER mechanism. Therefore, the use of abundant non-noble metals (Fe, Co, Ni, W, Mo, etc.) in place of noble metals for obtaining low-cost catalyst materials with high catalytic activity has become the focus of several studies on HER mechanism.

As a result of these studies, the most promising earth abundant catalysts that can replace Pt group noble metals have been determined as transition metal carbides (TMCs). Particularly the TMCs obtained using VIB group (Cr, Mo, W) atoms exhibit a catalytic activity in HER which is very close to Pt group. This is ascribed to the fact that, the interstitial Carbon (C) atoms retain the electrons from the metal atoms via charge transfer during TMC production by these atoms. As a result of this process, the altering electronic structure of metal atoms is assumed to contribute to the reduction in Tafel slope and overpotential values in HER mechanism [58]. The half of d orbitals of these metal atoms are full of electrons. Therefore, they have the configuration of an outer electron ($nd^5(n+1)s^1$). The electrons of these metals in d orbital are hybridized with 4 electrons ($2s^2\ 2p^2$) in the outer orbital of the Carbon

atom. As a result of this alteration, d orbitals of metal atoms are expanded and take on an electron configuration which is similar to that of Pt ($5d^9$ $6s^1$). Accordingly, the carbide structures of metals in HER exhibit a catalytic performance which is very similar to Pt [59].

Among the abovementioned substances W is in the same period (6th period) with Pt, therefore it has been the subject of studies on obtaining non-noble electrocatalysts for HER. The commonly used forms of W in HER are WC and W_2C. Tungsten carbides have similar band arrays with those of Pt. In addition, they are resistive against H_2S and CO intoxication [60]. In addition to the abovementioned TMCs, Tungsten carbides are also used as a supported material for Pt electrocatalysts. This way, the amount of noble metal can be reduced to reduce the costs [61-62]. Pure TMC and Pt loaded TMC structures of W, Mo, Cr are compared in Figure 2.7. As inferred from the figure, in pure TMC and Pt-loaded TMC structures, W carbides exhibit the lowest overpotential value, thereby displaying the best catalytic substance.

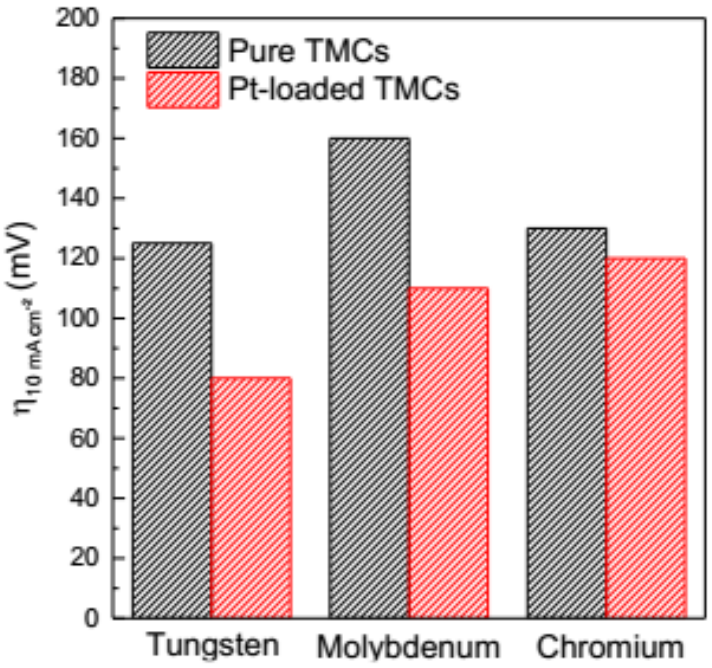


Figure 2.7 The comparison between the HER catalytic activities (the over-potentials at 10 mA cm^{-2}) of the VIB transition metal carbides and Pt-loaded carbides [58].

2.7 Literature Review

In 1950s, Bockris et *al.* found out that Pt has a very low activation energy for HER. The obtained findings showed that, Pt was a very good catalyst for HER [63-64].
In 1960s, WC was regarded as a candidate catalyst material due to its low cost and resistance against H_2S and CO intoxication [65]. Bianci et. *al.* pioneered the studies on use of tungsten carbide in HER [66].

Valance band theory was initially introduced by Engel Brewer in 1968. In this theory, some of the transition metal alloys (Co, W etc.) were proposed as efficient catalytic materials for HER owing to their specific d orbitals [67].

In 1973, R. B. Levy and M. Boudart reported that tungsten carbide has some catalytic characteristics similar to those of Pt. They attributed this to d-band electronic density states which are very similar to those of Pt [68].

Schroder et *al.* carried out a research on comparison of IVB and VIB transition metal compounds. In the research, borides, nitrides, carbides etc. samples were synthesized using similar industrial synthesis methods. In light of the findings, WC proved to be the sample with the best catalytic activity [69].

Meyer et *al.* used different transition metals in molten salt (KH_2PO_4) to compare the HER performance of these materials with that of Pt. The results obtained at 260°C showed that WC has a better catalytic activity than Pt [70].

Chen et *al.* used combustion carbo-thermal reduction method in WC_x/C synthesis for HER. The obtained research data showed that, the increase in C/W blocked the carburation and affected HER performance, in spite of the decrease in the grain size of WC [71].

Chaoyun et *al.* synthesized %20 Pt supported WC with hollow microsphere structure. HER performance of the obtained samples were evaluated. In conclusion, synthesis temperature and the number of active surface areas were reported to be important parameters for HER performance [72].

Liu Z. et *al.* for HER, WC @ C @ Pt has realized the catalyst synthesis in the double core shell structure by the half-combustion synthesis-carbonation (HCSC) method. The obtained results showed that these were among the best alternatives for W-supported Pt catalysts. The mesophorous structure of the obtained material was reported to be effective on this. In addition, it was also reported that, the depths of Pt particles embedded in Carbon could be kept under control during the carburization process [73].

Garcia-Esperza, Angel T., et *al.* synthesized WC nanowall as a catalyst for HER. A technique called direct current plasma assistant (DC-PACVD) was used as the synthesis method. It was reported on the basis of the experimental results that, WC nanowall catalyst was significantly resistive against the oxidation occuring during HER [74].

CHAPTER 3

EXPERIMENTAL STUDIES

3.1 Synthesis of Electrocatalyst Materials

Materials used in W, Pt and tungsten-platinum (W-Pt) NPs synthesis: Hexacarbonyltungsten (97%, $W(CO)_6$) was used in precursor material for W, Platinum(II) acetylacetonate (97%, $Pt(acac)_2$) was used as a precursor material for Pt. Oleic acid (99%, OA), oleylamine (70%, OLA), 1-octadecene (90%, ODE), chloroform (99.5%, $CHCl_3$), and ethanol (98%, EtOH) were bought from Alfa Aeser, UK. Graphite block (99.9%) used for electrode preparation was purchased from Beijing Great Wall Co, China.

3.1.1 Synthesis of Platinum (Pt) NPs

Pt NPs were synthesized under Ar atmosphere at ~200°C. 0.21g (0.534 mmol) $Pt(acac)_2$, 1 ml OA, 1 ml OLA and 10 ml ODE were added in a preaheated (120 °C) three-neck flask. The flask remained at this temperature up to $Pt(acac)_2$ was dissolved. Afterwards, the reaction mixture was heated up to 200°C gradually in 30 minutes and remained at that temperature for 30 minutes. The color change from clear to dark indicated the formation of Pt NPs. After the reaction was completed the flask was allowed to cool down to 80°C. A EtOH: $CHCl_3$ (30:5 ml). mixture was added into the resulting Pt NPs suspension. The obtained mixture was then centrifuged at 7000 rpm for 15 min. Following decantation, 5 ml $CHCl_3$ was added in the centrifuge tube to dissolve Pt NPs. The final precipitation was performed using 30 ml EtOH. The Pt NPs suspension was then centrifuged. After drying at 40°C we obtained 0.25 g of Pt NPs.

3.1.2 Synthesis of Tungsten (W) NPs

The synthesis of W NPs was performed under Ar atmosphere at ~230°C. In a synthesis 1.44 g (4.0 mmol) $W(CO)_6$, 0.22 g (2.0 mmol) OA, 1.06 (4.0 mmol) OLA and 25 ml ODE were added into a pre-heated (130°C) three-neck flask. The flask

remained at this temperature until $W(CO)_6$ dissolved. Afterwards, the reaction mixture was gradually heated to 230 °C in 10 minutes and held at that temperature for 1 hour. The formation of W NPs formation was indicated by the color change from clear to dark. After the reaction was completed the flask was allowed to cool down to 80°C. A mixture of EtOH: $CHCl_3$ (30:5 ml). was then added to the W NPs suspension obtained. Then the obtained mixture was centrifuged at 7000 rpm for 15 min. After precipitation 5 ml $CHCl_3$ was added in the centrifuge tube to dissolve W NPs. The final precipitation was done with 30 ml EtOH. The mixture of W NPs was centrifuged. After drying at 40°C we obtained 0.32 g of W NPs [75].

3.1.3 Synthesis of 5%Pt-W NPs

The synthesis of Pt-W NPs synthesis was conducted under Ar atmosphere at ~220°C. In a preaheated (130°C) three-neck flask were added 0.078g (0.198 mmol) $Pt(acac)_2$, 5ml ODE. The flask was held at this temperature until $Pt(acac)_2$ dissolved. After this step the temperature was increased gradually to 150°C and then were added 1.06 g OLA ,1.33 g (3,694 mmol) $W(CO)_6$,0.22g OA, 1 ml OLA and 20 ml ODE The mixture's temperature was gradually increased up to 220°C in 10 minutes, and held at this temperature for 1h. The formation of Pt-W NPs was indicated by the change in color from transparent to dark. When the reaction was completed, the flask was allowed to cool down to 80°C. A mixture of EtOH: $CHCl_3$ (30:5 ml) was then added into the obtained Pt NPs mixture. Then the Pt suspension was centrifuged at 7000 rpm for 15 min. To the obtained precipitate was added 5 ml $CHCl_3$. The final precipitation was done with 30 ml EtOH. The Pt-W NPs suspension was centrifuged twice at 7000 rpm for 15 min. After drying of the obtained powder at 40°C we weighted 0.30 g of Pt-W NPs

3.2 Preparation and Spin Coating of Electrodes

Graphite (C) was used as the electrode material. The electrodes were machined to the specified dimensions (nearly 45x15x2,5 mm). Following this process electrode surface was sandpapered and smoothened using FEPA # 500 abrasive. The graphite electrodes subjected to these processes are shown in Figure 3.1.

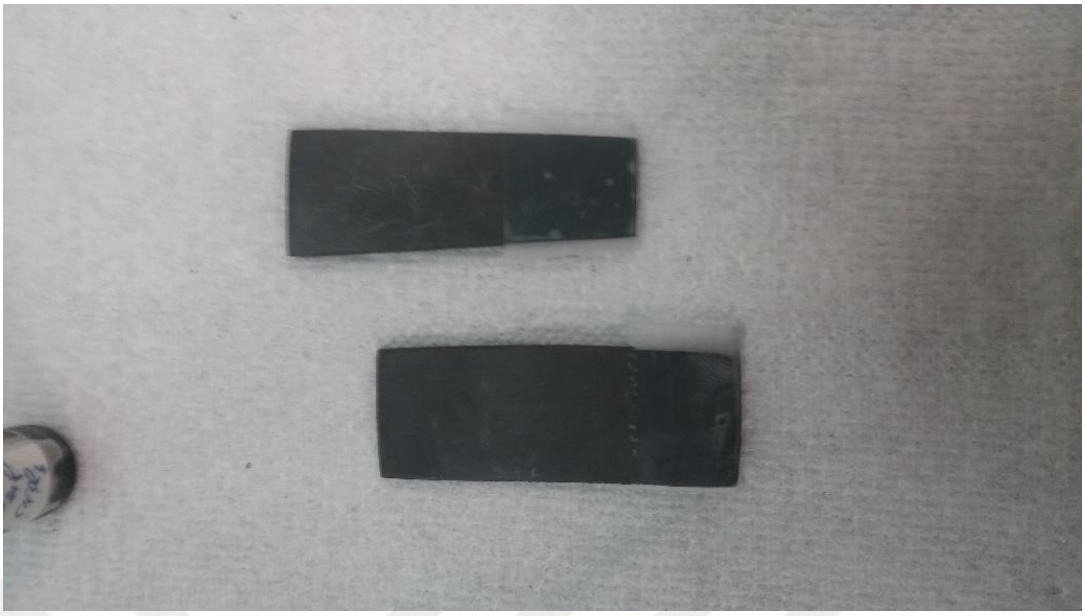


Figure 3.1 The prepared graphite electrodes

The electrodes were then coated with spin-coating process, which is a simple process widely used for surface coating of materials. The stages of spin coating process are shown in Figure 3.2. The process is based on the centrifugal principle. In this coating process, a fluid with resin viscosity is dropped onto the surface center of the material being coated. Following this process, it is spread on the substrate surface of the coating material by the aid of centrifugal force. Depending on the desired thin film thickness, the spin time and spin acceleration are modified. For instance, a very thin coating film can be obtained using high spin time and spin acceleration parameters.

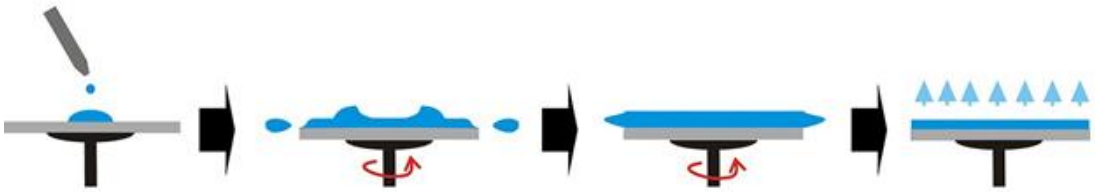


Figure. 3.2 Spin Coating Process [76].

After adding 2ml chloroform for obtaining the desired viscosity, the electrodes prepared for the coating process were subjected to spin coating with Pt and W as catalysts on a WS-400B-6NNP/LITE spin coater at 1000 rpm for a period of 20 s.



Figure 3.3 WS-400B-6NNP/LİTE Spin Coater.

3.3 Heat Treatment of Electrodes

Following the coating of electrodes using catalysts, heat treatment was applied on the electrodes. The detailed illustration of heat treatment process is given in Figure 3.4. Iron chips were used in the furnace as oxygen retainers to prevent oxidation of the electrode surfaces.

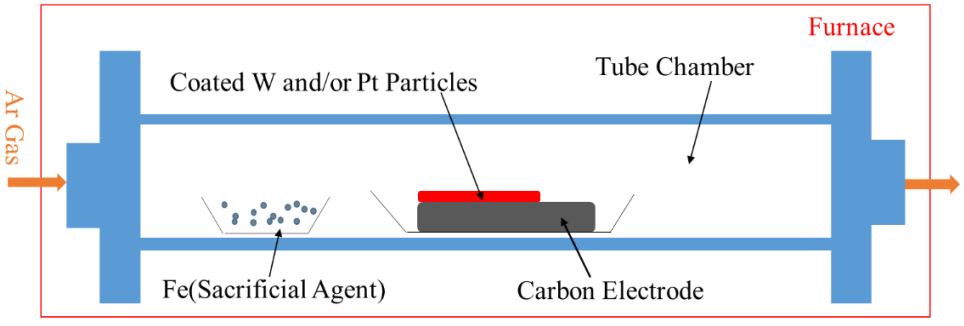


Figure 3.4 Heat treatment process.

Protherm brand heat furnace, shown in Figure 3.5, was used for the heat treatment process. The electrodes were subjected to heat treatment respectively at 900 °C, 1000°C, 1150°C, 1450°C for 150 minute under Argon (99,999%) atmosphere.



Figure 3.5 Protherm Heat Furnace

The electrodes subjected to coating and heat treatment are shown in Figure 3.6.



Figure 3.6 Electrodes of after heat treatments

3.4 Material Characterization Techniques

3.4.1 X-Ray Diffraction (XRD)

XRD is commonly used for characterization of metal thin films and powders. Rigaku Miniflex 600 (Oxford Instruments), shown in Figure 3.7, was used for XRD measurements in the present thesis study. In this method, collective characterization is performed instead of evaluation of surface sensitivity. XRD methods is also used for determination and definition of the structural characteristics of synthesized materials. By use of XRD method, it is determined whether the material is in metallic, carbidic or oxide structure, in addition to its surface orientation and crystal field dimensions [77].



Figure 3.7 Rigaku Miniflex 600 XRD

The working principle of X-Ray method is based upon the diffraction of light. When the light is scattered, diffraction is observed. In crystal structure, material atoms are organized in a repetitive and sequential order, which is known as lattice structure. In this method, an electromagnetic ray with a wavelength similar to the interatomic space between the atoms in the crystal structure, is used. The diffraction patterns resulting from the reflection of X-rays are used to gain information about the three

dimensional atomic packing of the material in crystal structure. The diffraction condition of the incident ray is defined with Bragg's law, as illustrated in Figure 3.8.

$$n\lambda = 2d\sin\theta \quad (3.1)$$

where, d is the distance between diffraction planes, θ is the scattering angle, λ is the wavelength of X-ray, and n is an integer.

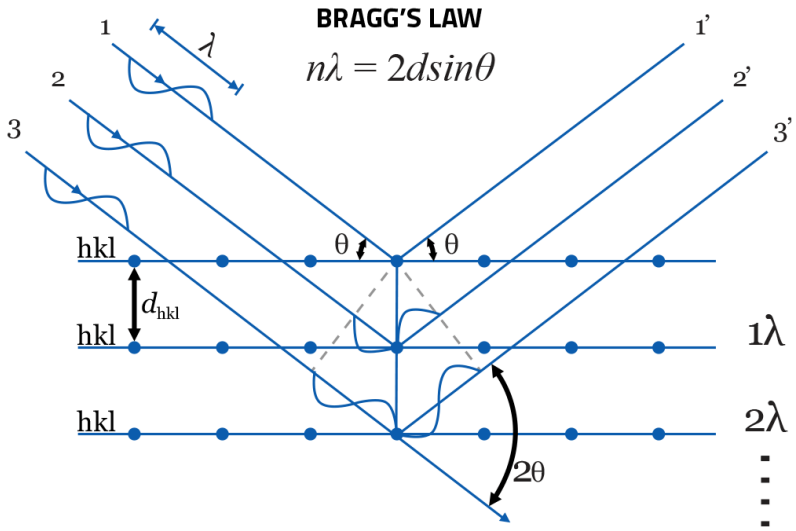


Figure 3.8 Bragg's Law [78].

3.4.2 Scanning Electron Microscopy (SEM)

Scanning electron microscopy is among the methods used to understand the physical characteristics of a material's surface. High resolution surface images of materials can be obtained using SEM technique. Focused electron beams with high energy are used to obtain SEM micrographs.

This method is generally used to obtain the micrographs of wide surface areas. Materials' surface topography, cristallinity and characterization of chemical composition are obtained with SEM. In this thesis study, SEM images were obtained using the Jeol JSM 7100F brand SEM which is shown in Figure 3.9.



Figure 3.9 Jeol JSM 7100F-SEM

3.4.3 Transmission Electron Microscopy (TEM)

TEM's working principle is similar to light microscope and as SEM, it uses focused electrons to obtain images. A synthesized material's chemical composition and crystal orientation can be determined using the obtained TEM images. TEM images vary depending on the density, thickness and composition of the analyzed material. For instance, materials with a low atomic number allow transmittance of more electron beams. This, in return, allows acquisition of brighter and clearer images as compared to those obtained from materials with a higher atomic number. Briefly, the working principle of a TEM device resembles a projector. The TEM images received in this thesis study was obtained the JEOL 2100F brand TEM device, as shown in Figure 3.10 [77, 79].

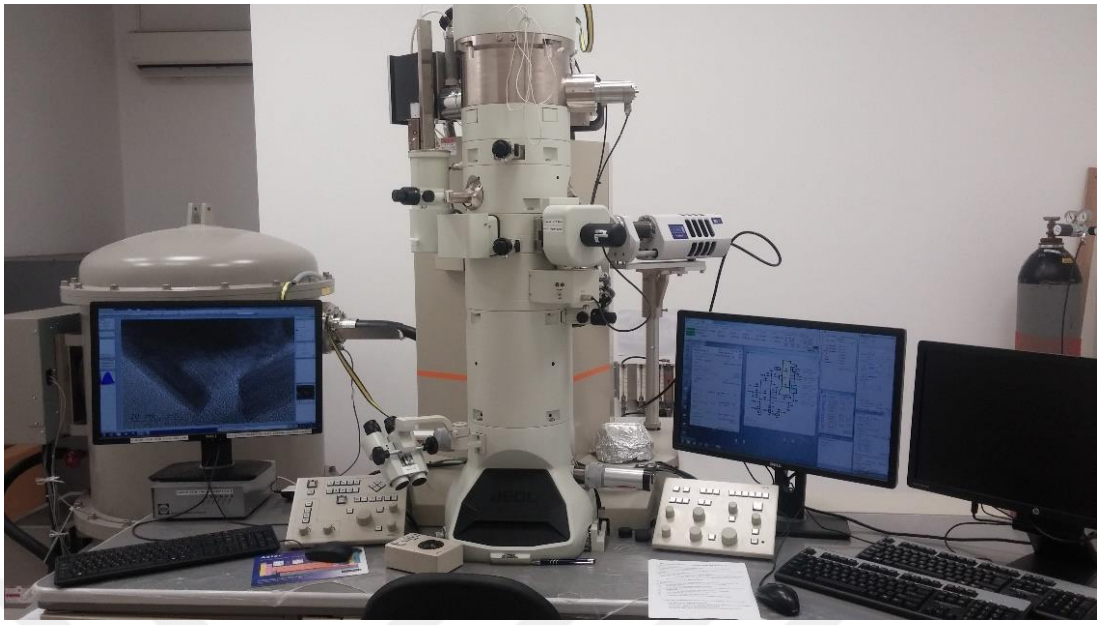


Figure 3.10 JEOL 2100F-TEM

3.4.4 Differential Scanning Calorimetry (DSC)

In this thesis study, DSC measurements were performed using TGA/DSC 2 Star System brand DSC device, which is shown in Figure 3.11.

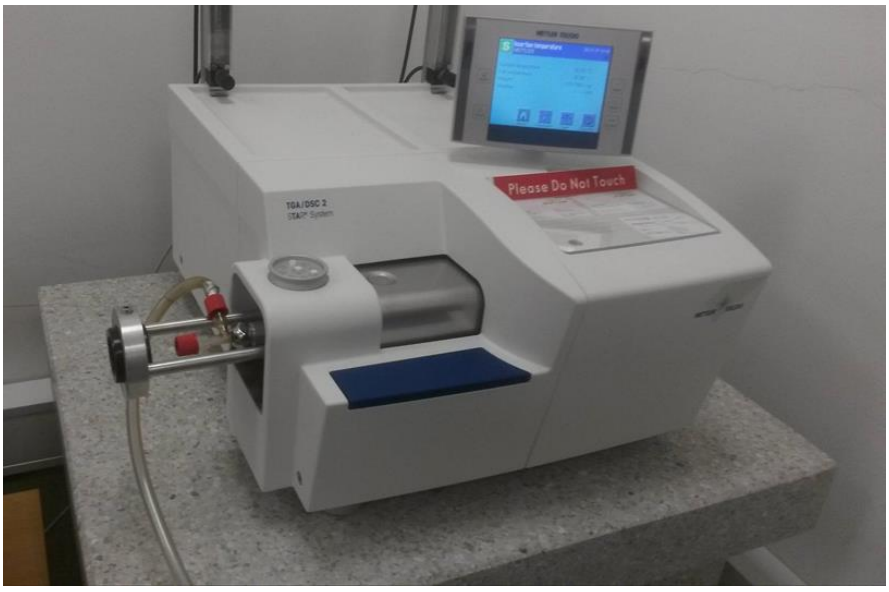


Figure 3.11 TGA/DSC 2 Star System

Differential Scanning Calorimetry (DSC) is a measurement technique for determination of the amount of heat required to increase the temperature for a sample and a reference material in a time dependent manner. The working principle of the system is shown in Figure 3.12.

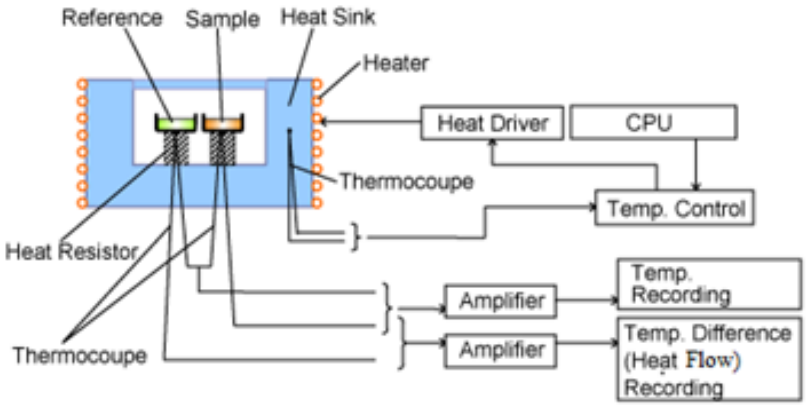


Figure 3.12 Working Process of DSC [Adapted from 80].

In this measurement method both the sample and the reference material are kept at the same temperature throughout the measurement. The difference between the heat flow of the sample and the reference material are then measured. The main principle is that, when the measured sample undergoes physical changes such as phase change, it requires higher or lower heat input than that of the reference material to keep up with its temperature. This situation varies depending on whether the process is endothermic or exothermic. For instance, during transition to the liquid phase, a solid sample will require higher heat flow and absorb the heat to keep up with the reference material's temperature. In such case, the process is endothermic. On the other hand, during crystallization, it will require less heat to keep up with the reference material's temperature, and dissipate heat (exothermic reacting). During such phase changes, the released or absorbed amount of heat can be measured by means of DSC. The material used as the reference material is usually an inert material (such as alumina) with a well-known heat capacity within the temperature interval of interest [81-82].

3.4.5 X-Ray Photoelectron Spectroscopy (XPS)

XPS is used to examine the surface chemistry of conductive or nonconductive materials. It is a surface-sensitive material characterization technique. The process takes place in a vacuum media to prevent inelastic collision of the scattered electrons with the molecules in gas phase. In this characterization technique, the sample surface being examined is subjected to X-rays (generally using Al or Mg). The measurement can be conducted at an approximate depth of ten nm. As the X-ray photons hit the metal surface, they transfer their energy to an electron at the core level. In such case, the electron is emitted with a kinetic energy that depends on the binding energy of the atomic orbit at the initial stage. The emitted electrons energy is then analyzed. The spectrum obtained comprise of the electrons at each energy interval and their kinetic energy. Each element has a specific spectrum [83-84]. In this study, XPS was performed to determine whether Pt was deposited onto the tungsten carbide samples during the electrochemical measurements conducted in the absence of Nafion.

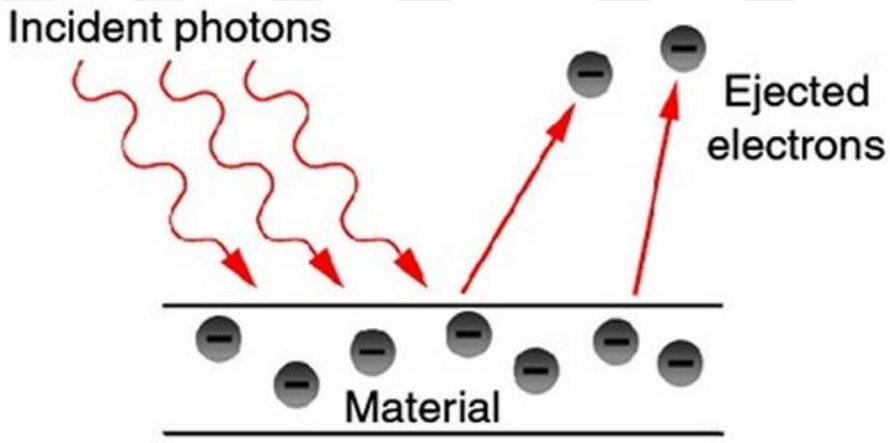


Figure 3.13 Photoelectric emission process of electrons [85].

3.5 Electrochemical Measurement Techniques

Following the characterization of materials used as catalysts, they were subjected to electrochemical measurement methods for determination of their stability and

activity. In this thesis study, the electrochemical measurements were performed with EDAQ SP1 model potentiostat, shown in Figure 3.14.



Figure 3.14 EDAQ SP1- Potentiostat.

Potentiostat is used to control the potential difference working electrode (WE) and reference electrode (RE). In this research, a Three-Electrode cell consisting of WE, counter electrode (CE), RE was used. In practice potentiostat measures the current flow between WE and CE. On a potentiostat, the controlled varying value is the cell potential, whereas the measured varying value is the cell current [86].

3.5.1 Three-Electrode Cell

In this thesis study, reduction (HER) half reaction was investigated instead of a comprehensive redox reaction. The activity of an electrode coated with an electrocatalyst in a reduction or oxidation reaction can be determined using a three-electrode cell. Also, half reactions, instead of a whole redox reaction, can be separately examined through the use of a three-electrode cell. As known, a three electrode cell ring involves 3 electrodes. These electrodes are respectively referred to as the working electrode (WE), reference elektrode (RE), and counter electrode (CE). WE is the electrode which is subject to the evaluation of catalyst characteristics. In

the system, WE is the electrode, potential and current values of which is to be measured. RE, on the other hand, is used to measure WE's potential. RE has a stable and well-known potential value. The current value, carried by RE electrode is supposed to be ideally zero. In this research a silver/silver chloride (Ag/AgCl- Sigma Aldrich) electrode was used as the RE electrode. CE electrode is the one which is used to complete the electrochemical cell circuit, and is generally chosen among inert conductive materials. In this research, Pt wire (99,999 %) was used as CE [86-87].

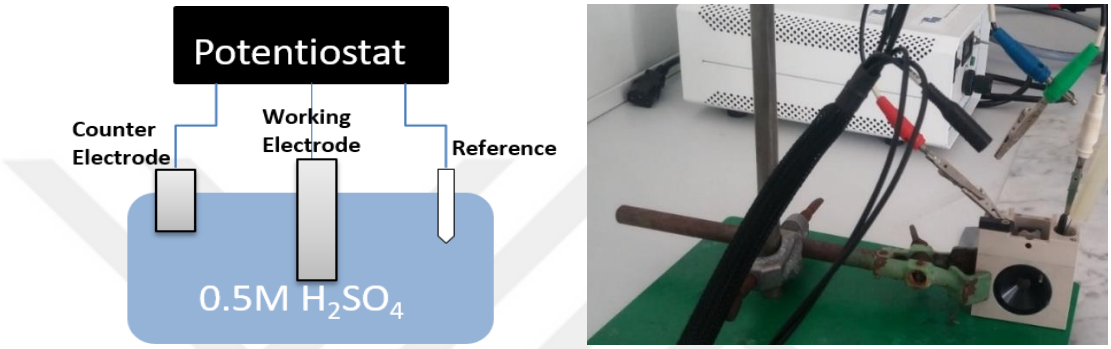


Figure 3.15 Three electrode configuration scheme (left) and a photo of the used cell (right)

In this study, 0.5 H_2SO_4 aqueous electrolyte (pH = 0) was used in electrochemical measurements. The electrode area of the electrochemical cell used is 0.283 cm^2. An O-ring was placed between the WE, which is in contact with the electrolyte, and the sample holder. The electrochemical cell shown in Figure 3.15 was used in the tests.

3.5.2 Linear Sweep Voltammetry (LSV)

LSV is one of the most commonly used electrochemical measurement methods. By use of this electrochemical measurement method, it can be determined whether the examined electrode (working electrode) is active with respect to HER or OER. In this technique, potential can be modified at a constant scan rate on the measured working electrode, thus scanning between the upper and lower potential values can be linearly performed as shown in Figure 3.17. Potential value linearly varies between the working electrode and the reference electrode, and at this instant the curent flow value throughout the working electrode is measured [88]. The results obtained from LSV are plotted as current vs. potential.

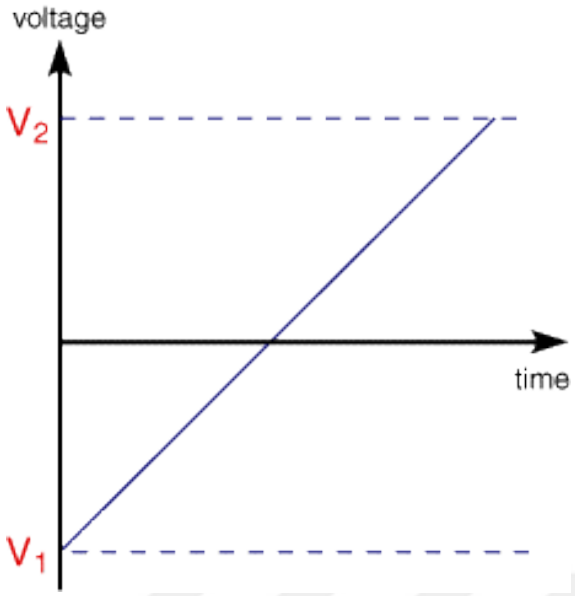


Figure 3.16 Ilustration of Linear Potential Sweep in LSV [89].

In this thesis study, LSV measurements were performed at 2 mV/s and 20mV/s scan rate values. The potential values of the plotted I-V graph was transformed into RHE using equation 2.5.

3.5.3 Electrochemical Impedance Spectroscopy (EIS)

EIS is an electrochemical method in which AC potential is applied on the subject system. EIS measurements are performed to determine the electrochemical system's limitations and develop the system performance. Electrochemical impedance can be defined as the reaction of the electrochemical system to the applied current or its frequency-dependant resistance. Impedance's dependency on the frequency enables understanding the internal elements of the chemical process that takes place in the system [90]. Impedance is denoted by Z_w and defined by the following formula:

$$Z_w=\frac{Ew}{Iw} \tag{3.2}$$

Where E_w is the frequency-dependent potential and I_w is the frequency-dependent current. Z has two values as real and imaginary as shown below:

Z_{real}, represents the resistance part of the impedance. No phase shift is observed between the voltage and current of a device with and Z has two values as real and imaginary.

$$Z_{total} = Z_{real} + Z_{imag} \quad (3.3)$$

Z_{real} represents the resistance part of the impedance. No phase shift is observed between the voltage and current of a device with a fully resistant impedance value. Z_{imag} constitutes the imaginary part of the impedance value. A device with a specified Z value undergoes phase shift between its voltage and current [91]. In this thesis, EIS measurements were carried out in the 3-electrode configuration at various potential from 0.0 to -0.2 V versus RHE and the frequency ranging from 10 μHz to 1 MHz with a 10 mV AC dither. EIS measurements, in this research, were performed to gain information about the charge transfer kinetics of the system.

CHAPTER 4

RESULTS AND DISCUSSION

4.1 Characterization Results of Pt, WC, W_2C

The platinum NPs used both to prepare the reference electrode are given in Figure 4.1. XRD measurement results of Platinum used as reference and dopping agent in this research are given in Figure 4.3. The TEM images indicate that the synthesized Pt atoms are polycrystalline since the electron diffraction forms well-defined rings. The interatomic planar space between Pt atoms was determined as Pt 0,225 nm in which correspond to (111) plane. It was also recorded the XRD diffractograms (not shown) of these Pt NPs which matches very well with a standard sample (PDF: 1011107). The size of synthesized Pt NPs was found to vary between sizes 2 to 5 nm.

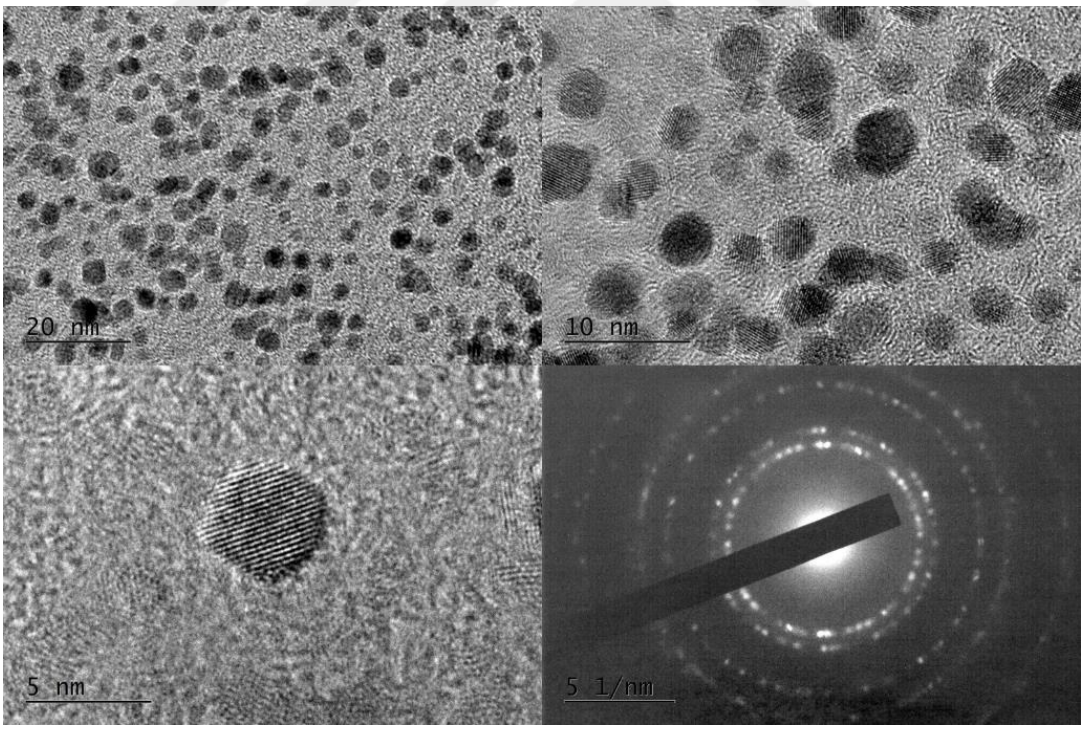


Figure 4.1 TEM images of synthesized Pt nanomaterials at different magnifications and diffractograms (lower right) taken from the object in shown in upper right corner.

TEM images of W NPs are shown in Fig. 4.2. Due to its irregular atomic packing, W NPs before heat treatment are in amorphous phase as shown in the electron diffractogram. The lack of sharp diffraction rings in the diffractogram indicate that the material is in amorphous state. The W NPs are extremely small with sizes below 3 nm in diameter. Since they are amorphous and small the obtain TEM contrast is also low.

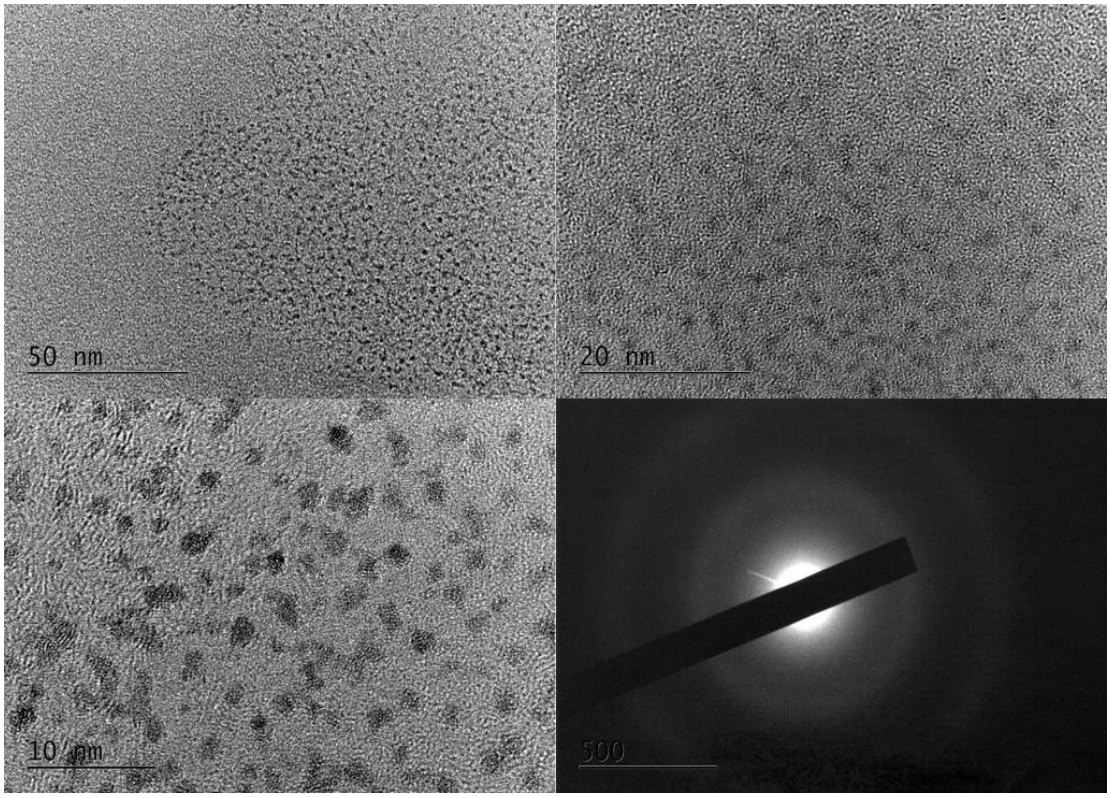


Figure 4.2 TEM images of synthesized W nanomaterials

Figure 4.2. shows diffractograms of tungsten and tungsten carbide phases prepared at different heat treatment temperatures. W thin films were subjected to heat treatment at 900°C, 1000°C, 1150°C and 1450°C under Ar atmosphere.

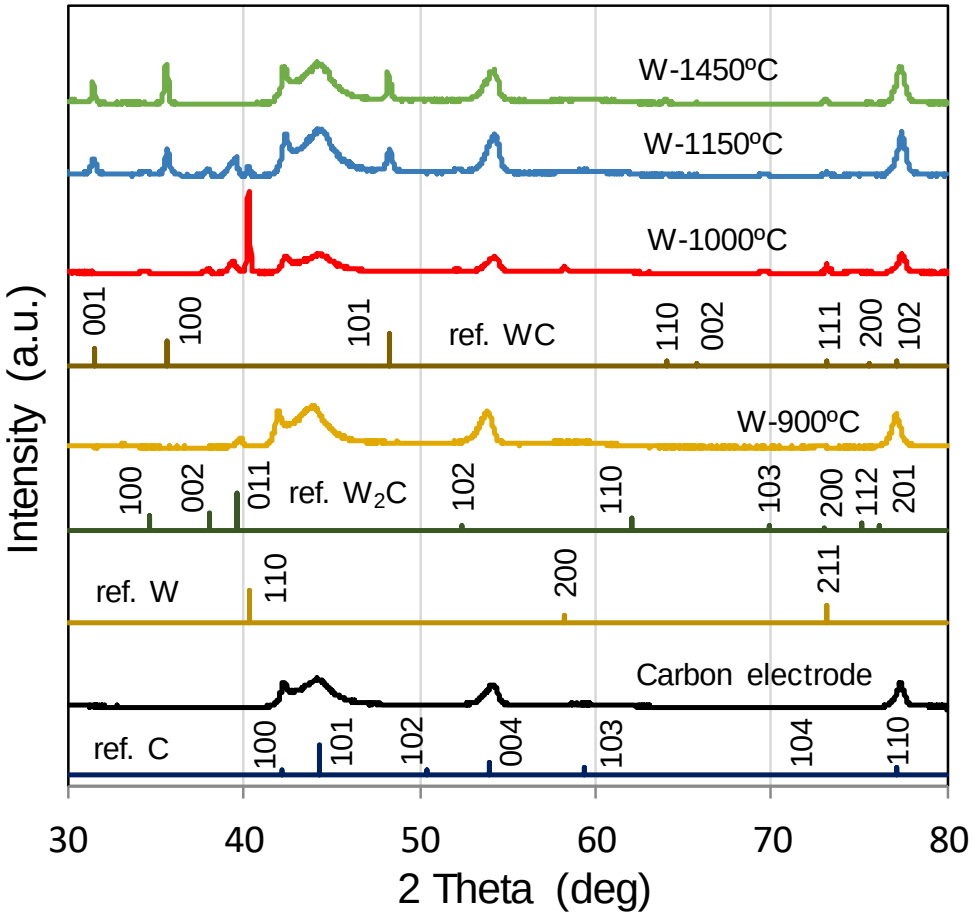


Figure 4.3 XRD patterns of W, W_2C, WC and their mixed phases. Reference patterns of W, W_2C and WC are given with labels [92].

In the W sample heat treated at 900°C the small diffraction peak at 39.6°C was attributed to metallic W (PDF: 9006487). After increasing the temperature to 1000°C the peak for metallic W shifted to 40.34°. Moreover, this peak also increased its intensity indicating that at this temperature occurred accelerated crystallization of the amorphous W phase resulting in metallic W NPs with sizes between 50 nm to 300 nm (Fig. 4.5). This increase in crystallization also results in an increase in W peak. At 1000°C it also started formation of W_2C phase (PDF: 5910041).

Formation of WC phase was observed following the heat treatment on W at 1150°C. Mixture of W: W_2C: WC phases coexisted on the sample heated up to 1150°C. The mixture ratios of these phases were respectively found as 9.4:11.4:79.2% using Referance Intensity Ratio (RIR) method [93]. Pure WC phase was obtained

following the heat treatment applied at 1450°C (PDF:2100636). Tungsten carbide formation occurred on W surface in the presence of metallic W and active carbon (C*) [94]. The diffusion of active carbon yields W_2C or WC phase depending on the heat treatment temperature.

The DSC curve of a typical W sample is shown in Figure 4.4. DSC measurements were performed at N_2 atmosphere by heating W sample from 50°C to 1500°C. The sample used in DSC measurement was obtained via mixing W, NPs and carbon powders. The peak point represented with (i) approximately indicates the loss of organic molecules such as steric acid oleylamine molecules (covering W NPs) at 460°C. The next instant transition point abbreviated as (ii) emerged at 900°C as shown in the Figure 4.4. This peak point corresponds to an endothermic reaction such as the melting of W NPs. The melting point of bulk tungsten is known as 3422°C. However, in the case of metallic NPs can be observed at low temperatures as well [95]. The small peak (reverse) abbreviated as (ii) is most probably corresponds to W NPs melting.

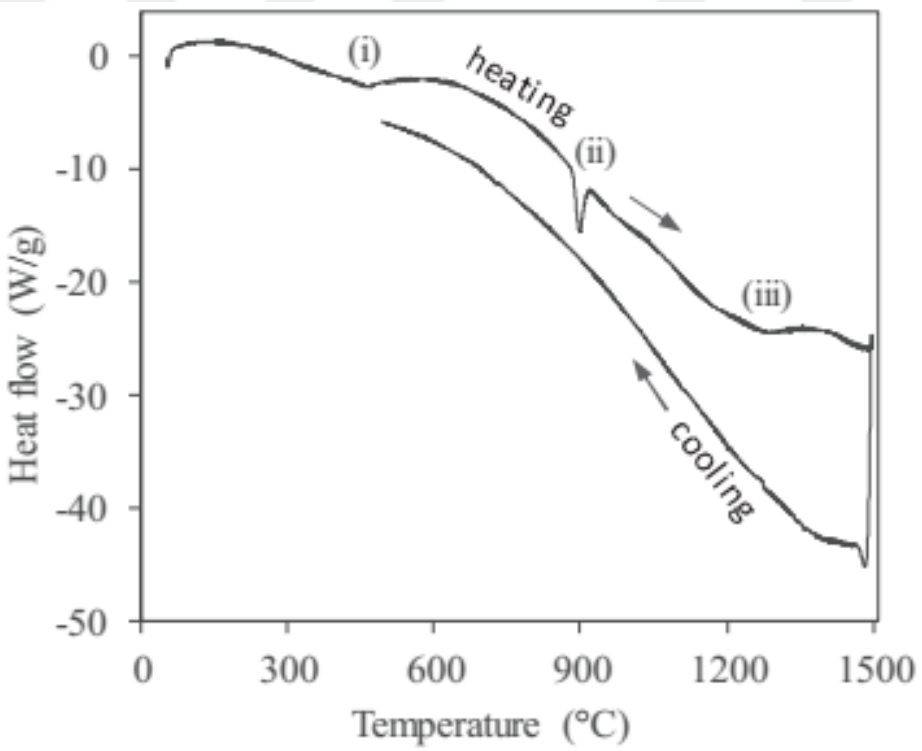


Figure 4.4 DSC curves of W sample heat treated with a ramp 20 °C/min under N_2 atmosphere [92].

The crystallization which cannot be observed on the DSC curve is an exothermic reaction. However, endothermic melting reaction of W NPs in amorphous structure was observed during the continuous heat flow experiment. Another peak point on the DSC curve, represented with (iii), is likely to be associated with the tungsten carbide formation which arose at 1280°C. Transformation of metallic W NPs into WC phase was observed at high temperatures, while no peak indicating the crystallization of W NPs was observed on the DSC curve during the cooling process.

The graphite film heat treatment at 900°C after the coating process (with graphite and W NPs) is shown in Figure 4.5. As shown in the figure, the non-heat treated graphite surface is relatively smoother. However, porous structures with diameters exceeding >3μm were observed on the graphite surface (coated with W) NPs which was heat treated at 900°C and coated with W NPs with diameters ranging from 50-300 nm. As shown in Figure 4.5 b-c, the W NPs-coated graphite surface exhibits a crystal structure as indicated on the XRD plot (Figure 4.3).

W NPs coating on the graphite surface was subjected to Energy Dispersive Elemental (EDS) analysis to examine its distribution on the surface. The W map, obtained using the same sample is shown in Figure 4.5 d, e (c). The overlapping of SEM images and W map is given in Figure 4.5 e. The small objects shown in yellow color are metallic W NPs. It is clearly indicated in the EDS map that W NPs is evenly distributed on the graphite surface. The peaks of C and W elements are shown in the EDS spectrum in Figure 4.4. The higher intensity of the signals obtained for C element in the EDS spectrum is attributed to the substrate's being made of graphite. belonging to C and W elements are shown in the EDS spectrum in Figure 4.4. The higher intensity of the signals obtained for C element in the EDS spectrum is attributed to the substrate's being made of graphite, hence the higher signal intensity of C element, as compared to W.

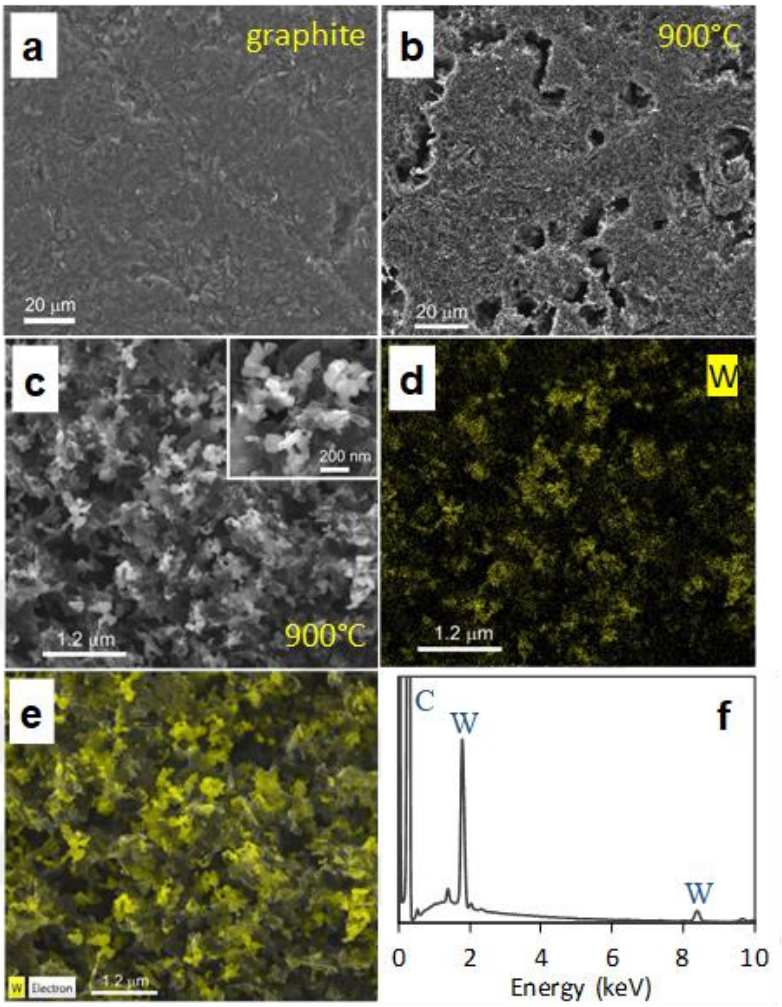


Figure 4.5 SEM images of (a) pure graphite and (b-e) W NPs coated graphite substrates prepared at 900°C. In (d-f) are given images with elemental maps for W taken from the object shown in (c). The image in (e) is an overlay of W map with (c). Magnified image of W NPs (white objects) is given as an inset in (c). In (f) is given the spectrum used to construct the maps [92].

The SEM images of the W NPs heat-treated at 1000°C, 1150°C and, 1450°C are shown in Figure 4.6. The homogeneous distribution of W and C is clearly indicated on the SEM images Moreover, EDS analysis of the sample prepared at 1150°C reveals homogeneous distribution of W element (Figure 4.6 d). The average diameter of the tungsten formations following the above-mentioned heat treatments was found to increase with increasing temperature. The diameters of NPs in the sample obtained after heat treatment at 1000°C varied between 40-300 nm whereas those of the NPs on the sample subjected to heat treatment at 1450°C exceeded 500 nm. In addition, the sample obtained after heat treatment at 1450°C resulted in WC NPs with lower

loads. It can be inferred that the WC NPs in the sample have lower densities due to their bigger sizes. As a result, the surface areas of these WC NPs are also expected to be smaller.

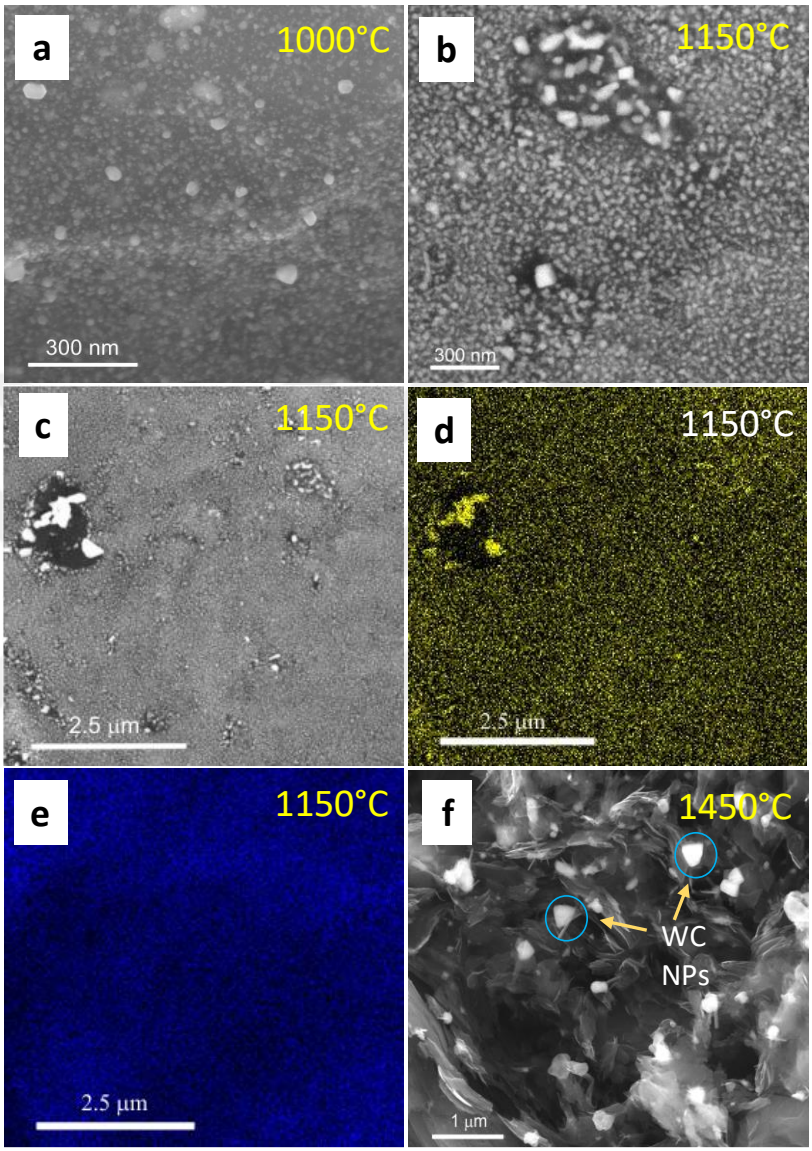


Figure 4.6 SEM images of W samples heat treated at (a) 1000°C, (b) 1150°C, and (f) 1450°C. In (c) is given an SEM image and elemental maps for (d) W and (e) C of W sample prepared at 1150°C. The scale bars: (a,b) 300 nm, (c-e) 2.5 µm and (f) 1 µm [92].

It was also synthesized Pt doped W NPs which were used for the preparation of Pt doped W or Pt doped W_2C thin films. The Pt dopant concentration was kept at 5% (w/w) with respect to tungsten precursor. The preparation steps for Pt doped W films were similar as described for the pure W thin films. It was prepared two sets of Pt

doped W samples which were obtained after at 900°C and 1150°C. The SEM images of these samples are shown in Figure 4.7 and Figure 4.8. EDS analyses on both samples showed that W and Pt exhibited a homogeneous distribution on the graphite substrate. Additionally, the presence of Pt is quite clear at the locations where is W. The morphology of the objects resembles a more to a net-like formations rather than individual NPs.

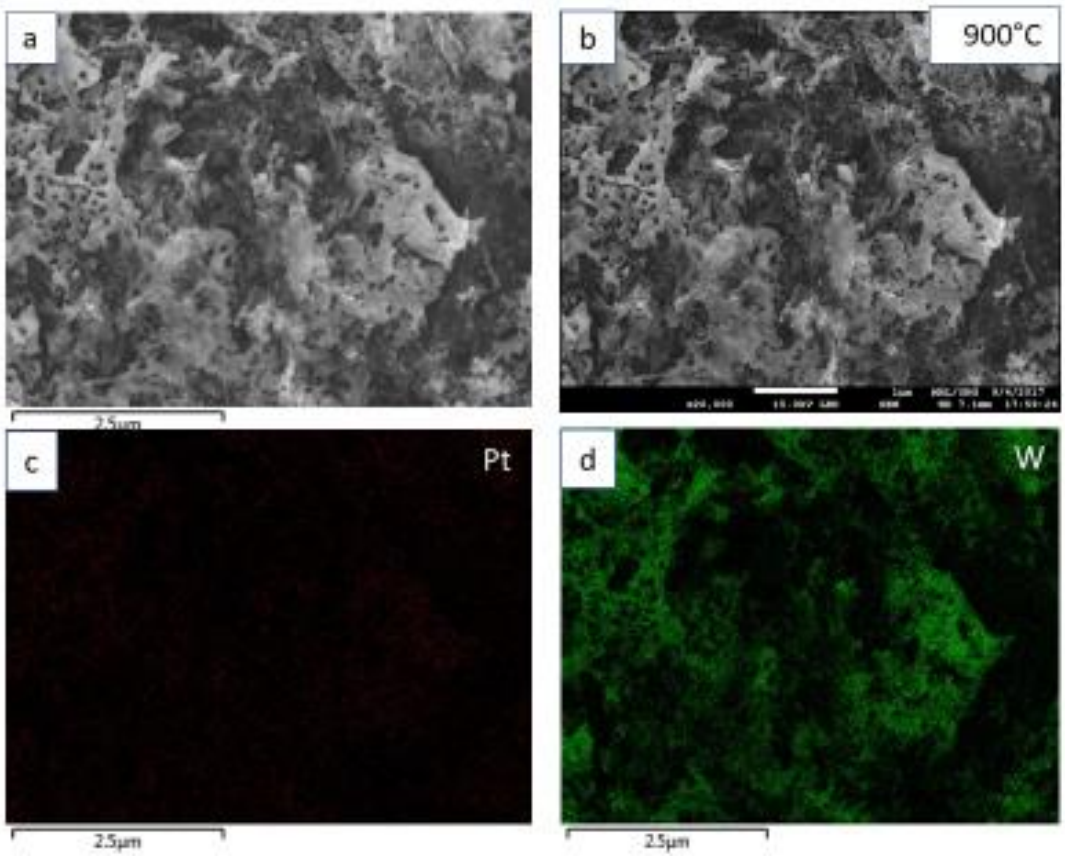


Figure 4.7 In (a), (b), SEM images of 5%Pt-W samples heat treated at 900°C. (c), (d) is elemental maps for Pt and W respectively. The scale bars: (b) 1 µm, (a, c, d) 2,5 µm.

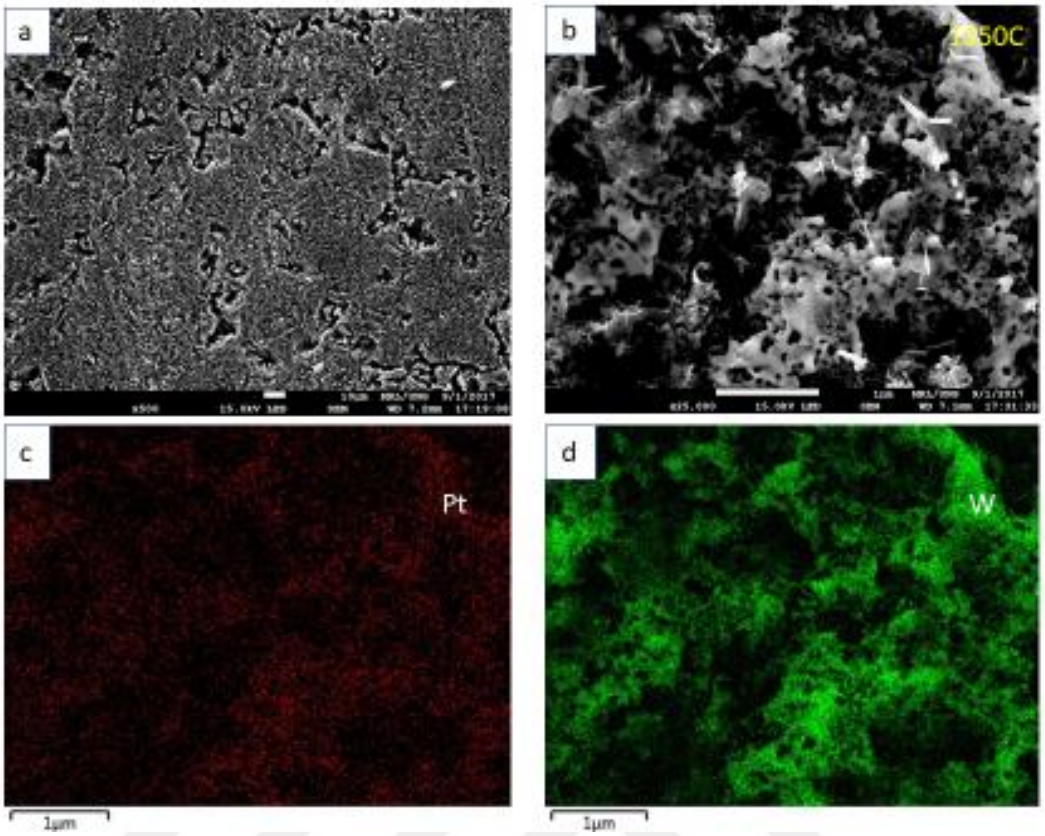


Figure 4.8 In (a), (b), SEM images of 5%Pt-W samples heat treated at 1150°C. (c), (d) is elemental maps for Pt and W respectively. The scale bars: (a) 10 µm., (b, c, d) 1 µm.

The TEM images of WC nanosheet prepared after the heat treatment at 1450°C is shown in Figure 4.9. The WC nanosheet was found to be a single crystal as shown in the electron diffractogram. The dimensions of WC nanosheet is over 500 nm. High magnified TEM image of the WC nanosheet is shown in Figure 4.9b. The interplanar spacing is 0.253 nm which correspond to (100) plane.

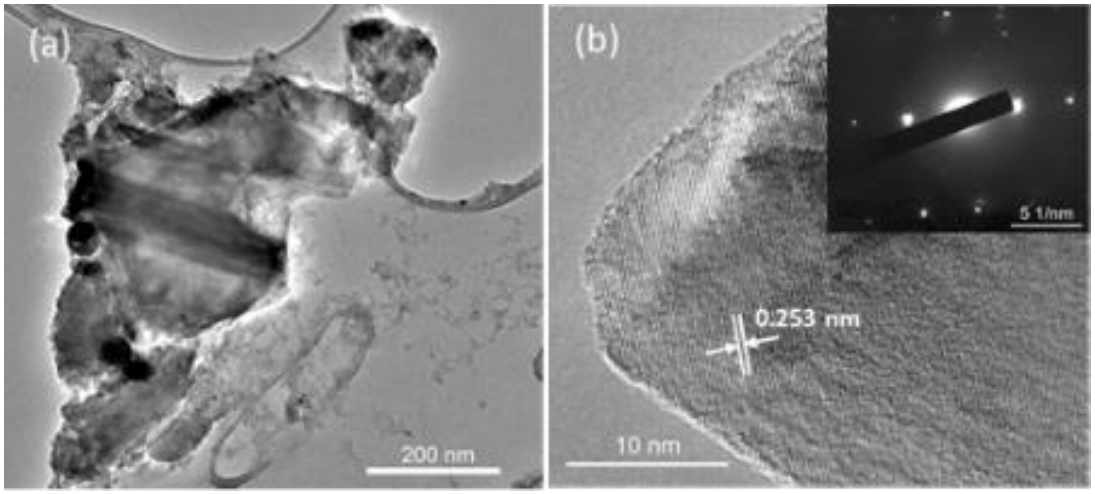


Figure 4.9 (a, b) TEM image of WC nanosheet at different magnifications. The inset in (b) is an electron diffraction image [92].

4.2 Electrochemical Measurement Results

4.2.1 Linear Sweep Voltammetry and Stability Test

The catalytic HER performance of the tungsten-based samples was examined in 0.5 M H_2SO_4 following the heat treatment of samples at 900°C, 1000°C, 1150°C and 1450°C. As the most important parameters of catalytic performance, obtained after the experimental studies, LSV and Tafel plots are given in Figure 4.10. As clearly indicated on the LSV graph in Figure 4.10 (a), the HER performance of graphite is at a negligible level. Likewise, as shown in Figure 4.10 (a), the lowest overpotential value was obtained from the sample which was subjected to heat treatment at 1150°C. The overpotential (η_{10}) for the samples were determined at the current density value of 10 mA/cm^2. The η_{10} value corresponding to this value was determined as 310 mV. The η_{10} value found for Pt/C, used as the reference material, is 110 mV. However, η_{10} value of the Pt/C catalysts used in the literature studies can be as low as 35 mV [96].

In this research, the higher overpotential value of Pt/C as compared to the literature is due to the quality of Pt NPs on graphite. The performance of Pt NPs is not optimized and that is why the overpotential is high. The η_{10} values determined for the remaining samples are W900°C-296 mV, W1450°C-384 mV and W1000°C-389 mV, as shown

in Figure 4.10 (a). For better interpretation of the reaction mechanism is presented Tafel plot as shown in Figure 4.10(b). The data are shown in potential vs logj (current density in logarithm) [74, 97]. It is clearly indicated that the W sample heat treated at 1150°C exhibit small Tafel slope of 108 mV/dec. It can be inferred that the reaction steps followed for HER performance are those of the Volmer-Hyrovsky mechanism. Another important parameter provided by Tafel slope is the rate determining step, which is useful for evaluation of the HER performance of the catalyst material which is used as electrode.

This research involved Volmer rate determining step. Tafel slope gives descriptive information for comparison of the kinetic rate of the proton discharge reaction that occurred at the Volmer rate determining step. From the viewpoint of HER performance, a material used as catalyst is expected to exhibit a low Tafel slope value. In light of this information, W (heat treatment at 1150°C) was found to exhibit the best catalytic activity among the examined samples.

A catalyst, which is to be used for HER, is expected to have a good stability. The stability tests of tungsten carbide thin films obtained at 1150°C were performed in 0.5M H_2SO_4 with and without Nafion117. The overpotential was found to decrease to 310 mV from 268 mV during the stability test performed without Nafion 117 (Figure 4.10, c). However, the fluctuation in overpotential value was averted with the stability test performed using Nafion 117 (Figure 4.10, d). Therefore, our material is very stable under these time window tested.

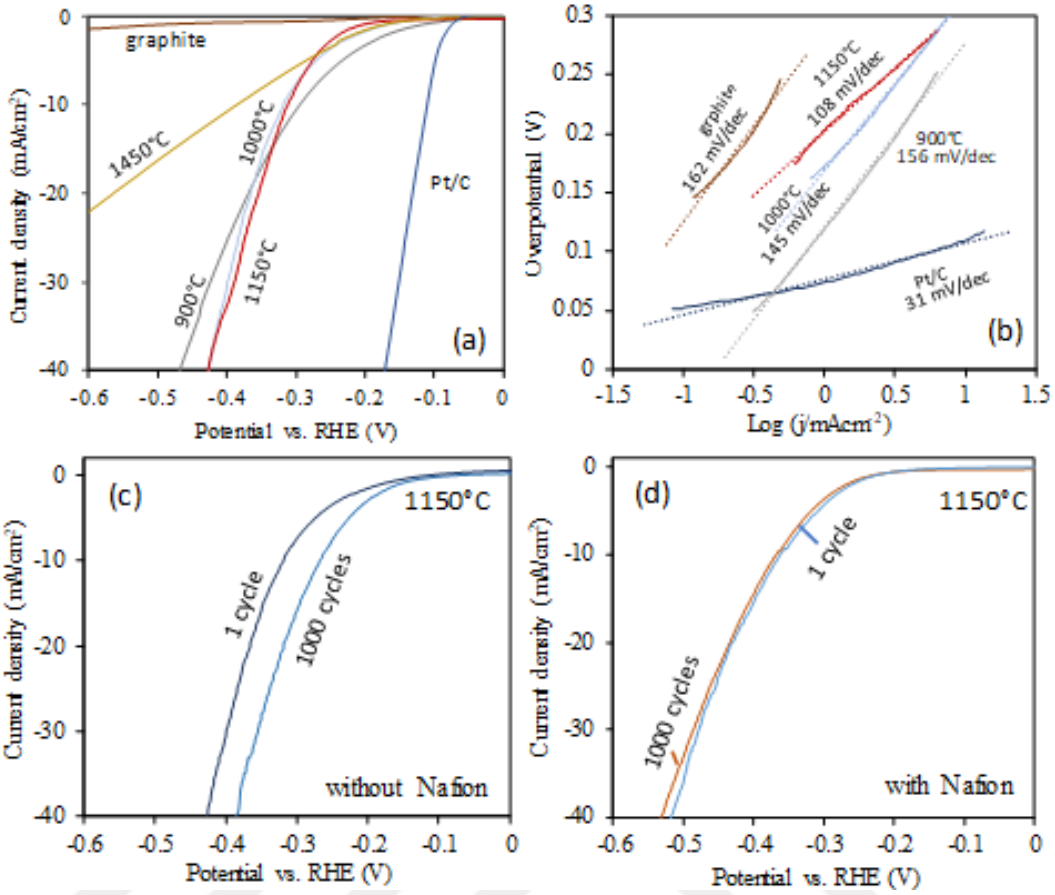


Figure 4.10 (a) Polarisation curves of W/C films heated treated at different temperatures (one compartment cell). The linear sweep voltammograms are recorded in 0.5 M H_2SO_4 with a scan rate of 2 mV/s. The reference Pt-C electrode is prepared by coating Pt NPs on graphite. In (b) are given Tafel plots for the different electrodes. Polarisation curves of the sample heat treated at 1150°C (c) without and (d) with Nafion membrane after the 1-st and 1000-th cycles [92].

In various studies, tungsten carbide was used as support material for Pt loadings [98]. In this research, Pt doped (5% w/w) W films were prepared for the purpose of achiving efficient HER. An original synthesis method was used to prepare colloidal Pt-W NPs. The obtained bimetallic Pt-W NPs were spin-coated on graphite and heat treated at 900°C and 1150°C. The composition of the films is mainly Pt-W (900°C) and Pt-W/W_2C/WC (1150°C). The HER activity of the Pt modified tungsten carbide thin films obtained after the heat treatment step were evaluated in 0.5M H_2SO_4.

The LSV and Tafel Plot of the samples are shown in Figure 4.11. As indicated in the LSV graph in Figure 4.11 (a), the lowest overpotential value was obtained from the

sample subjected to heat treatment at 1150°C. The η_{10} value for this sample was found as 154 mV. The η_{10} value of the Pt modified tungsten carbide sample prepared at 900°C was found as 143 mV. The Tafel slopes given in Figure 4.11 (b) are 118 mV/dec (1150°C) and 152 mV/dec (900°C).

The Tafel values indicate that the reaction steps followed in the HER activity is Volmer-Heyrovsky, similar to W-1150°C samples. The LSV slopes obtained for the Pt modified tungsten carbide samples show reduced the overpotential for HER compared to pure tungsten carbide samples.

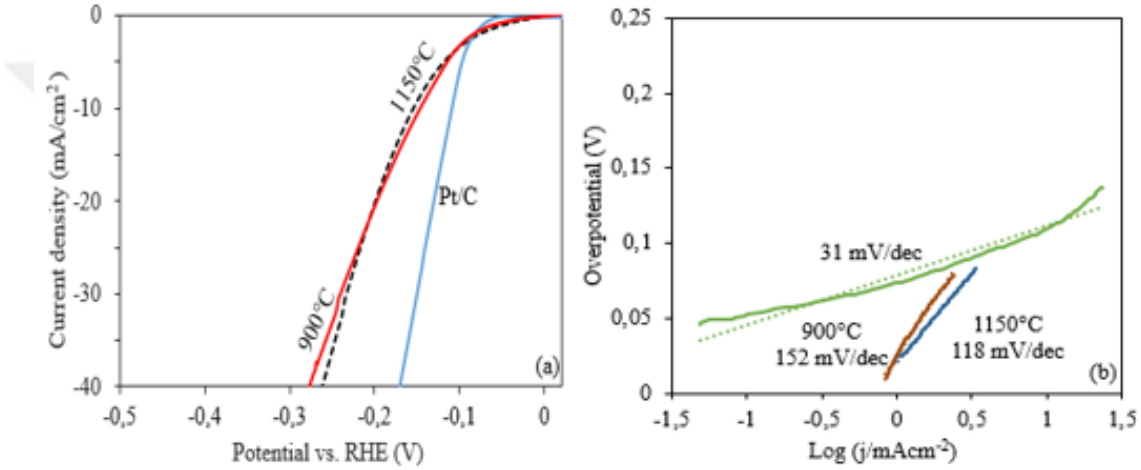


Figure 4.11 (a) Polarisation curves of 5%Pt-W/C films heated treated at different temperatures (one compartment cell). The linear sweep voltammograms are recorded in 0.5 M H_2SO_4 with a scan rate of 20 mV/s. In (b) are given Tafel plots for the different electrodes.

Table 4.1 Promising tungsten based carbides used in HER studies [74, 96, 99-104, 106-110]

Material	Loading (mg/cm^2)	Tafel slope (mV/dec)	η_0 (mV)	η_{10} (mV)	Solution
WC NPs (~5 nm)	~0.98	84	N/A	~125	0.5 M H_2SO_4
W_2C NPs (~2 nm)	0.209	49	N/A	51	0.5 M H_2SO_4
W_xC/graphene oxide NPs	0.14	58.4	N/A	100	0.5 M H_2SO_4
WC/WN	2.2 − 10	36	N/A	105	0.1 M $HClO_4$
W_2C/graphene	2.2	65	N/A	120	0.1 M $HClO_4$
WC/graphene	0.002	38	N/A	120	0.5 M H_2SO_4
WMoC nanowires	1.28	82	N/A	~135	0.5 M H_2SO_4
WC nanowire	N/A	75	~20	~150	0.5 M H_2SO_4
WC nanowall	N/A	N/A	52	160	0.5 M H_2SO_4
CoWC	~0.28	75 mV	N/A	200	0.5 M H_2SO_4
WC nanocrystalline	N/A	N/A	102	248	0.5 M H_2SO_4
WC	~0.71	N/A	165	~250	0.5 M H_2SO_4
WC_x/C	1.05	85	N/A	264	0.5 M H_2SO_4
WC NPs	N/A	122	N/A	489	0.05M H_2SO_4
W NPs **(this study)**	~2.7	156	N/A	295	0.5 M H_2SO_4
W_2C/WC NPs **(this study)**	~2.7	108	N/A	310	0.5 M H_2SO_4

To compare our results with the literature data we made a short summary of the overpotentials recorded for tungsten carbide systems (Table 4.1). Xu et al., has reported one of the best performing tungsten carbide (WC) catalyst with η_{10} − 51 mV [96]. They have shown that small WC NPs (~2 nm) offer this outstanding catalytic performance. The Tafel slope extracted from the polarisation curve is also as low as 49 mV/dec approaching the value ~35 mV/dec reported for Pt-C catalyst. This clearly indicates that the crystalline phase and particle morphology of the material used as catalyst has a very significant effect on the HER performance [100]. The trend in Table 4.1 is very clear, catalysts with high activity for HER exhibit low overpotential and small Tafel slope, athough, the recorded overpotentials are higher than the literature reports for the best systems. This difference is attributable to the differerent synthesis methods used to obtain electrocatalysts. It can be expected that sizes of catalyst NPs, attachment of the catalysts to the substrate, crystal defects in the catalyst and also ratio of different phases are among the factors that contribute to the catalytic properties.

Heat treatment duration is one factor which greatly affect the composition of samples (different phases). Chen et al. reported that W/C ratio is a determining factor for the HER performance of the catalytic material [71]. As in the case of other

electrocatalytic materials obtained from transition metals, the HER performance of tungsten catalyst materials is dependent on the number of their active regions. It can be accordingly stated that, W/C ratio and catalyst surface termination could greatly HER performance.

Table 4.1, some of the reported tungsten carbides applied for HER. The best results are obtained in a system with very small NPs sizes (e.g. 2 nm). Small NPs sizes bring high surface area and a homogeneous distribution over the substrate [111].

This study comes useful in showing the relation between synthetic protocol and catalytic activity of materials. Obviously, the best performing systems are made of tungsten carbides with small sizes. In our case, our starting precursor is made of very small (2-4 nm) W NPs. However, during the heat treatment steps these W NPs sinter into larger particles which eventually does not yield catalysts with low (<100 mV) overpotential. In this thesis, the differences in the best catalytic HER performances displayed by W-900°C and W-1150°C is ascribed to the difference in their composition. In one case we have only pure W NPs (900°C) and in the other case mixture of phases like W/W_2C/WC (1150°C). Although the W-900°C sample display good overpotential (<300 mV) at 10 mA/cm^2, it does not show higher activity for HER at higher current densities (e.g. 50 mA/cm^2). This finding indicates that WC and W_2C display a better catalytic HER performance as compared to pure W phase.

Table 4.2 Tungsten supported Pt used in HER studies[72,73,105, 112]

Material	**Tafel slope (mV/dec)**	η_0 **(mV)**	η_{10} **(mV)**	**Solution**
20 % Pt/WC (hollowmicrosphere)	27.1	22	N/A	0.5 M H_2SO_4
Double core shall WC@C@Pt	26	9	30	0.5 M H_2SO_4
7.5wt%Pt/W_2C	103	5	N/A	1 M H_2SO_4
Pt/WC powder microelectrode	124	N/A	250	0.5 M H_2SO_4
5%Pt-W NPs **(this study)**	152	28.7	143	0.5 M H_2SO_4
5%Pt- W_2C/WC NPs **(this study)**	118	37.6	154	0.5 M H_2SO_4

Table 4.2 was prepared with a view to compare the results obtained from the W supported Pt electrocatalysts with literature results. Liu Z. et al. has reported one of the best performing W supported Pt catalysts with η_{10} 30 mV [73].

In their study, the mesoporous structure of the catalyst material (average-3,76 nm) was determined as one of the leading factors underlying this remarkable result, as the mesoporous structure promoted the diffusion of the electrolyte, which in turn facilitated the reaction kinetics [113]. The obtained sample's Tafel slope (26 mV/dec) is better than that of the Pt/C catalyst. The material synthesized in this study demonstrated satisfactory results. The overpotential is higher than the best system reported in the literature. However, the dopant concentration is low and is still not optimized for HER. To improve the system is needed to test different dopant concentration and check which heat treatment is more suitable. The protocol in which was used for the preparation of Pt-W_2C/WC films is original which in principle could allow tuning various parameter for better optimization.

Electrochemical impedance spectroscopy (EIS) was conducted at different overpotentials to investigate the underlying electrochemical activity of the synthesized catalysts. Nyquist type plots at different applied potentials are shown in Figure 4.12. The recorded impedance signal decreases with the applied overpotential. EIS data were modelled with an equivalent circuit element as shown in the inset in Figure 6b. In this model, contact phase (CPE) and resistance (R) elements connected in series are used. The charge transfer-resistance (R_{ct}) obtained from the semicircle at low frequencies is related to the kinetics of HER process while the smaller semicircle at high frequencies corresponds to the medium's ohmic resistance. Th decrease in R_{ct} with the applied overpotential arises from the faster charge-transfer kinetics (Figure 4.12 b).

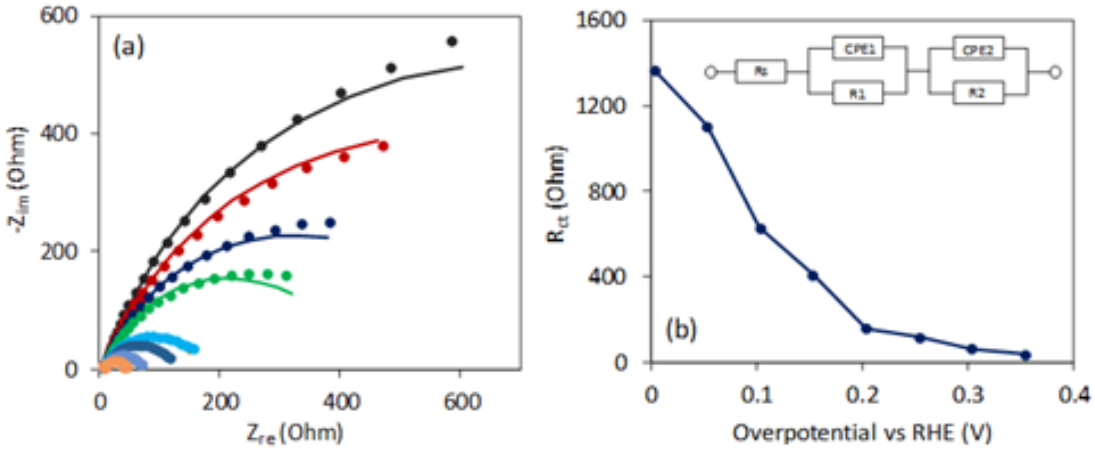


Figure 4.12 Nyquist plot of W1150°C in 0.5M H_2SO_4 recorded with a bias from 0.0 to 350 mV. In (b) is given the charge-transfer resistance (Rct) vs overpotential. Inset is given an electrical equivalent circuit used to fit the EIS data [92].

4.2.2 XPS Measurement Results

X-ray photoelectron spectroscopy (XPS) studies are performed to address the reduction in overpotential observed in Figure 4.10 c. Figure 4.13 shows survey spectrum of W-1150°C sample obtained after the stability test without Nafion 117 membrane. The characteristics spectral lines of Pt 4f are given in Figure 4.13b. The two peaks with 71.2 and 75 eV binding energies are assigned to Pt 4f7/2 and Pt 4f5/2.

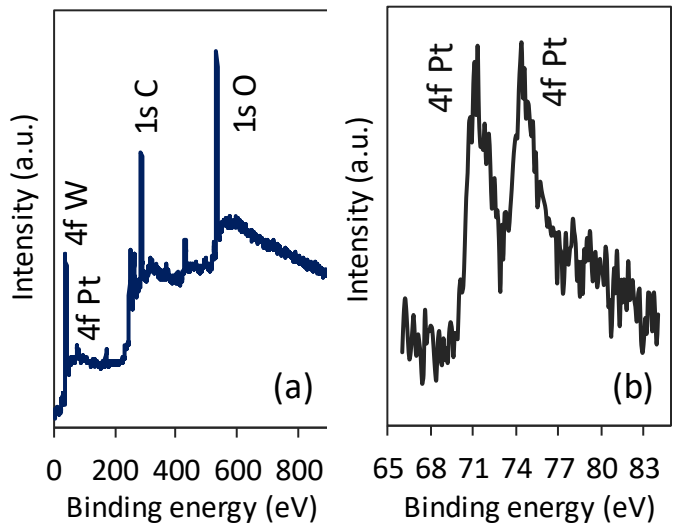


Figure 4.13 XPS data of W1150°C film recorded after the stability test for 1000 cycles without Nafion 117 membrane. (a) Wide spectra and (b) 4f Pt signals.

The two peaks correspond to the metallic Pt NPs deposited on the surface of the tungsten carbide electrode during the stability tests. In acidic media under applied potential, Pt metal (e.g. counter electrode) can easily dissolve to yield Pt^{2+} ions which are reduced on the working electrode (e.g. tungsten carbide). The unintentional electro-deposition of Pt on the working electrode has been proposed as one factor for improved HER performance of this sample. To avoid deposition of Pt on the working electrode can be taken two measures. One approach is to replace the Pt electrode with more robust material like graphite. The other approach is to use a cell with two compartments which are devided by a Nafion membrane. The aim of the Nafion membrane is to avoid migration of Pt^{2+} ions from the compartment where is located the Pt counter electrode toward the working electrode area. It is well known that Nafion membranes conducts only H^{+} which is sufficient to allow to support ionic conductivity between the two electrodes and promote HER.

CHAPTER 5

CONCLUSIONS

The present thesis study was carried out to investigate hydrogen production by using electrochemical water splitting. Tungsten carbide and Pt doped tungsten carbide were synthesized for use as electrocatalyst for HER. Colloidal W and Pt-W NPs were used to prepare W, W/W_2C, W/W_2C/WC, WC, Pt/W and Pt/W_2C/WC thin films on graphite electrodes after heat treatment at different temperatures. Structural and morphological characterization of the thin films were carried out by XRD, XPS, TEM and SEM. Electrocatalytic activities of the thin films were evaluated using LSV and EIS. In the case of undoped W samples the best HER performance was achieved with the samples heat treated at 1150°C. It was found that this sample contain mixture of phases such as W, W_2C and WC. Moreover, the obtained findings were compared with the available literature studies.

The best sample in this study showed 310 mV overpotential for HER. A good stability was observed after 1000 cycles.

In the case of Pt doped tungsten carbide samples, the best ovepotential was 154 mV at pH=0. Moreover, the applied charge-transfer resistance (R_{ct}) was examined via the EIS measurements. The calculated R_{ct} value indicates that R_{ct} decreases with the applied potential. In this thesis, it has been successfully demonstrated a facile method for synthesis of colloidal W NPs which find application for preparation of tungsten carbide films. The obtained tungsten carbide thin films were used for H_2 generation using electrolysis of water. The thesis paves the road for preparation of earth-abundant and low-cost electrocatalyst materials for HER.

REFERENCES

[1] Acar, C. & Dincer, I. “Impact assessment and efficiency evaluation of hydrogen production methods”. *International journal of energy research*, *39*(13), 1757-1768, 2015

[2] Dincer, I., & Acar, C. “Review and evaluation of hydrogen production methods for better sustainability”. *International journal of hydrogen energy*, *40*(34), 11094-11111, 2015

[3] Hydrogen. (n.d). Retrieved February 16, 2018, from http://www.rsc.org/periodic-table/element/1/hydrogen

[4] The Element Hydrogen. (n.d). Retrieved February 16, 2018, from https://education.jlab.org/itselemental/ele001.html

[5] Momirlan, M., & Veziroglu, T. N. “The properties of hydrogen as fuel tomorrow in sustainable energy system for a cleaner planet”. *International journal of hydrogen energy*, *30*(7), 795-802, 2005

[6] Delikanlı, K., Bayhan, M., & Jankowski, A. “Hidrojenin Motorlarda Kullanımı ve Motor Gürültüsüne Etkisi”. *Mühendis ve Makina* 49, 582, 2005

[7] Balat, M. “ Potential importance of hydrogen as a future solution to environmental and transportation problems”. *International journal of hydrogen energy*, *33*(15), 4013-4029,2008

[8] Hydrogen Basics Production. (n.d). Retrieved February 16, 2018, from http://www.fsec.ucf.edu/en/consumer/hydrogen/basics/production.htm

[9] Zou, X., & Zhang, Y. “Noble metal-free hydrogen evolution catalysts for water splitting”. *Chemical Society Reviews*, *44*(15), 5148-5180, 2015

[10] Abdin, Z., Webb, C. J., & Gray, E. M. “Solar hydrogen hybrid energy systems for off-grid electricity supply: A critical review”. *Renewable and Sustainable Energy Reviews*, *52*, 1791-1808.2015

[11] TRASATTI, S. “Water electrolysis: who first?” *Journal of Electroanalytical Chemistry*, 476.1: 90-91, 1999

[12] Li, X., Hao, X., Abudula, A., & Guan, G. “Nanostructured catalysts for electrochemical water splitting: current state and prospects”. *Journal of Materials Chemistry A*, *4*(31), 11973-12000, 2016

[13] Kreuter, W., & Hofmann, H. “Electrolysis: the important energy transformer in a world of sustainable energy”. *International Journal of Hydrogen Energy*, *23*(8), 661-666, 1998

[14] J. O’M. Bockris, B. E. Conway, and E.(Ed.) Yeager, *Comprehensive Treatise of Electrochemistry. Volume 2: Electrochemical Processing*.(1st ed.) New York: Plenum Press, 1981

[15] E. Gileadi, *Electrode Kinetics for Chemical Engineers and Material Scientists*, VCH, London, 1993.

[16] Bard, A. J., Faulkner, L. R., Leddy, J., & Zoski, C. G. *Electrochemical methods: fundamentals and applications* (Vol. 2). New York: Wiley. 1980

[17] Zoulias, E., Varkaraki, E., Lymberopoulos, N., Christodoulou, C. N., and Karagiorgis, G. N. “A review on water electrolysis”. *Tcjst, 4(2),* 41-71.2004

[18] Nocera, D.G. “Chemistry of personalized solar energy”. *Inorganic chemistry*, *48*(21), 10001-10017, 2009

[19] Ursua, A., Gandia, L. M., & Sanchis, P. “Hydrogen production from water electrolysis: current status and future trends”. *Proceedings of the IEEE*, *100*(2), 410-426, 2012

[20] Chase, M. W. NIST—JANAF *Thermochemical Tables. Journal of Physical and Chemical Reference Data Monograph No. 9*. (Fourth Edition). Maryland: American Institute of Physics, 1998.

[21] Roger, I., Shipman, M. A., & Symes, M. D. "Earth-abundant catalysts for electrochemical and photoelectrochemical water splitting". *Nature Reviews Chemistry, 1*(1), 0003, 2017

[22] Durst, J., Siebel, A., Simon, C., Hasche, F., Herranz, J., & Gasteiger, H. A. "New insights into the electrochemical hydrogen oxidation and evolution reaction mechanism". *Energy & Environmental Science, 7*(7), 2255-2260, 2014

[23] Zhu, W. Amine Promotion of hydrogen evolution reaction suppression and carbon dioxide conversion for artificial photosynthesis. Unpublished doctoral dissertation, University of Illinois at Urbana-Champaign, 2011

[24] Wahl, D. "A Short History of Electrochemistry- Part I". *Galvanotechnik, 96(7),* 1600-1610, 2011

[25] The Nernst Equation. (n.d). Retrieved February 28, 2018, from https://chem.libretexts.org/Textbook_Maps/General_Chemistry_Textbook_Maps/Map%3A_Chem1_(Lower)/16%3A_Electrochemistry/24.04%3A_The_Nernst_Equation

[26] Pourbaix Water. (n.d). Retrieved February 28, 2018, from https://upload.wikimedia.org/wikipedia/commons/1/1d/PourbaixWater.png

[27] Buendía-Delgadillo, T., Delgadillo-Núñez, F., Casillas, N., Ibanez, J. G., & Barcena-Soto, M. "Construction of a Novel Reversible Hydrogen Electrode (RHE)". *The Chemical Educator, 16,* 326-328, 2011

[28] Roger Barba, I. Investigations into electrochemical water splitting. Unpublished doctoral dissertation, University of Glasgow, 2017

[29] Hoang, S., Guo, S., Hahn, N. T., Bard, A. J., & Mullins, C. B."Visible light driven photoelectrochemical water oxidation on nitrogen-modified TiO_2 nanowires". *Nano letters*, *12*(1), 26-32, 2011

[30] Conway, B. E., & Gileadi, E. "Kinetic theory of pseudo-capacitance and electrode reactions at appreciable surface coverage". *Transactions of the Faraday Society*, *58*, 2493-2509, 1962

[31] Yang, Y. Design and Preparation of Novel Electrocatalysts for Oxygen Evolution Reaction. Unpublished doctoral dissertation, The University of Qeensland, 2017

[32] Yang, T.Tuning the hydrogen evolution activity of beta phase Mo2C nanoparticles via control of their growth conditions. Unpublished doctoral dissertation, University of Pittsburgh, 2017

[33] Electrolysis. (n.d). Retrieved February 28, 2018, from https://courses.lumenlearning.com/wsu-sandbox2/chapter/electrolysis/

[34] Colombo, A.L.E.S.S.A.N.D.R.A.. Preparation and Performance Evalution of Materials for Electrocatalytic Applications. Unpublished doctoral dissertation, UNIVERSITÀ DEGLI STUDI DI MILANO, 2010

[35] Cook, T. R., Dogutan, D. K., Reece, S. Y., Surendranath, Y., Teets, T. S., & Nocera, D. G."Solar energy supply and storage for the legacy and nonlegacy worlds". *Chemical reviews*, *110*(11), 6474-6502, 2010

[36] Wang, A.. Study on Nanostructured Molybdenum Carbide for Hydrogen Evolution Reaction. Unpublished doctoral dissertation, University of Pittsburgh, 2017

[37] Zeng, K., & Eng, M. Improvements and Optimisation of Water Electrolysis for Hydrogen Production. Unpublished doctorla dissertation University of Western Australia, 2012

[38] Thuv, H.The Oxygen Evolution Reaction at Iridium-Ruthenium Oxide Catalysts for PEM Water Electrolysis. Unpublished master's thesis, NTNU, 2015

[39] Shan-Shan, T. O. N. G., Xue-Jing, W. A. N. G., Qing-Chuan, L. I., & Xiao-Jun, H. "Progress on Electrocatalysts of Hydrogen Evolution Reaction Based on Carbon Fiber Materials". *Chinese Journal of Analytical Chemistry*, *44*(9), 1447-1457, 2016

[40] Stern, M., & Geary, A. L.Electrochemical polarization I." A theoretical analysis of the shape of polarization curves". *Journal of the electrochemical society*, *104*(1), 56-63, 1957

[41] Chen, W. F., Muckerman, J. T., & Fujita, E. "Recent developments in transition metal carbides and nitrides as hydrogen evolution electrocatalysts". *Chemical communications*, *49*(79), 8896-8909, 2013

[42] Gileadi, E. *Electrode kinetics for chemists, chemical engineers, and materials scientists.* New York: Wiley-VCH, March, 1993.

[43] Bagotsky, V. S. *Electric Currents in Ionic Conductors. Fundamentals of Electrochemistry*,(2nd Ed.) New Jersey: John Wiley & Sons, 2006.

[44] Santos, D. M., Sequeira, C. A., & Figueiredo, J. L. "Hydrogen production by alkaline water electrolysis". *Química Nova*, *36*(8), 1176-1193, 2013

[45] Goor, C. Influence of temperature and pH on the hydrogen evolution reaction (HER) on platinum. Bachelor's thesis, University of Twente, 2015

[46] Li, Y., Wang, H., Xie, L., Liang, Y., Hong, G., & Dai, H. "MoS_2 nanoparticles grown on graphene: an advanced catalyst for the hydrogen evolution reaction". *Journal of the American Chemical Society*, *133*(19), 7296-7299, 2011

[47] Sohail, M. G.. Corrosion of steel in concrete: development of an accelerated test by carbonation and galvanic coupling. Unpublished doctoral dissertation, Université de Toulouse, Université Toulouse III-Paul Sabatier, 2013

[48] Greeley, J., Jaramillo, T. F., Bonde, J., Chorkendorff, I. B., & Nørskov, J. K. Computational high-throughput screening of electrocatalytic materials for hydrogen evolution. *Nature materials*, *5*(11), 909, 2006

[49] Tang, Q., & Jiang, D. E. "Mechanism of hydrogen evolution reaction on 1T-MoS_2 from first principles". *Acs Catalysis*, *6*(8), 4953-4961, 2016

[50] Gibbs Free Energy. (n.d). Retrieved February 28, 2018, from http://chemed.chem.purdue.edu/genchem/topicreview/bp/ch21/gibbs.php

[51] De Pauli, C. P., & Trasatti, S. "Composite materials for electrocatalysis of O_2 evolution: IrO_2 + SnO_2 in acid solution". *Journal of Electroanalytical Chemistry*, *538*, 145-151, 2002

[52] Bonde, J. L. New Materials for Hydrogen Evolution. Unpublished doctoral dissertation Technical University of Denmark, 2008

[53] Avcu, F.. Atık sulardaki fenolün elektrooksidasyon ile arıtılması için elektroaktif elektrot geliştirilmesi. Unpublished master's thesis, Çukurova Üniversitesi, 2010

[54] Pletcher, D., Greff, R., Peat, R., Peter, L. M., and Robinson, J., *Instrumental Methods in Electrochemistry*, Philadelphia: Woodhead Publishing, 2001.

[55] Sapountzi, F. M., Gracia, J. M., Fredriksson, H. O., & Niemantsverdriet, J. H.. "Electrocatalysts for the generation of hydrogen, oxygen and synthesis gas". *Progress in Energy and Combustion Science*, *58*, 1-35, 2017

[56] Conway, B. E., & Tilak, B. V.. "Interfacial processes involving electrocatalytic evolution and oxidation of H_2, and the role of chemisorbed H". *Electrochimica Acta*, *47*(22-23), 3571-3594, 2002

[57] Skúlason, E., Tripkovic, V., Björketun, M. E., Gudmundsdóttir, S., Karlberg, G., Rossmeisl, J., et al. “Modeling the electrochemical hydrogen oxidation and evolution reactions on the basis of density functional theory calculations”. *The Journal of Physical Chemistry C*, *114*(42), 18182-18197, 2010

[58] Zhao, X., Yin, F.X., He, X., & Chen, B.. “Recent Progress in Transition Metal Carbide Electrocatalysts for the Hydrogen Evolution Reaction”. *Research & Reviews in Electrochemistry, 8(1),* 105, 2017

[59] Kitchin, J. R., Nørskov, J. K., Barteau, M. A., & Chen, J. G..”Trends in the chemical properties of early transition metal carbide surfaces: A density functional study”. *Catalysis Today*, *105*(1), 66-73, 2005

[60] Stellwagen, D. R., & Bitter, J. H.. “Structure–performance relations of molybdenum-and tungsten carbide catalysts for deoxygenation”. *Green Chemistry*, *17*(1), 582-593, 2015

[61] Kelly, T. G., Lee, K. X., & Chen, J. G.. “Pt-modified molybdenum carbide for the hydrogen evolution reaction: From model surfaces to powder electrocatalysts”. *Journal of Power Sources*, *271*, 76-81, 2014

[62] Kelly, T. G., Hunt, S. T., Esposito, D. V., & Chen, J. G.. “Monolayer palladium supported on molybdenum and tungsten carbide substrates as low-cost hydrogen evolution reaction (HER) electrocatalysts”. *international journal of hydrogen energy*, *38*(14), 5638-5644, 2013

[63] Bockris, J. M., & Conway, B. E.. “The velocity of hydrogen evolution at silver cathodes as a function of hydrogen ion concentration”. *Transactions of the Faraday Society*, *48*, 724-730, 1952

[64] Bockris, J. M., & Azzam, A. M.. “The kinetics of the hydrogen evolution reaction at high current densities”. *Transactions of the Faraday Society*, *48*, 145-160, 1952

[65] Harnisch, F., Schröder, U., Quaas, M., & Scholz, F.. ”Electrocatalytic and corrosion behaviour of tungsten carbide in near-neutral pH electrolytes”. *Applied Catalysis B: Environmental*, *87*(1-2), 63-69, 2009

[66] Bianchi, G., Mazza, F., & Trasatti, S.. “Aynodic behavior and passivity of some interstitial compounds of niobium, tantalum, titanium, and tungsten”. *Z. phys. Chem*, *226*, 40-58, 1964

[67] Zheng, H., Huang, J., Wang, W., & Ma, C.. “Preparation of nano-crystalline tungsten carbide thin film electrode and its electrocatalytic activity for hydrogen evolution”. *Electrochemistry communications*, *7*(10), 1045-1049, 2005

[68] Levy, R. B., & Boudart, M.. “Platinum-like behavior of tungsten carbide in surface catalysis”. *science*, *181*(4099), 547-549, 1973

[69] Wirth, S., Harnisch, F., Weinmann, M., & Schröder, U.. “Comparative study of IVB–VIB transition metal compound electrocatalysts for the hydrogen evolution reaction”. *Applied Catalysis B: Environmental*, *126*, 225-230, 2012

[70] Meyer, S., Nikiforov, A. V., Petrushina, I. M., Köhler, K., Christensen, E., Jensen, et al.. “Transition metal carbides (WC, Mo_2C, TaC, NbC) as potential electrocatalysts for the hydrogen evolution reaction (HER) at medium temperatures”. *international journal of hydrogen energy*, *40*(7), 2905-2911, 2015

[71] Chen, Z., Qin, M., Chen, P., Jia, B., He, Q., & Qu, X.. “Tungsten carbide/carbon composite synthesized by combustion-carbothermal reduction method as electrocatalyst for hydrogen evolution reaction”. *International Journal of Hydrogen Energy*, *41*(30), 13005-13013, 2016

[72] Tang, C., Wang, D., Wu, Z., & Duan, B..”Tungsten carbide hollow microspheres as electrocatalyst and platinum support for hydrogen evolution reaction”. *International Journal of Hydrogen Energy*, *40*(8), 3229-3237, 2015

[73] Liu, Z., Huo, X., Xi, K., Li, P., Yue, L., Huang, M., et al. “Thickness controllable and mass produced WC@C@Pt hybrid for efficient hydrogen production”. *Energy Storage Materials*, *10*, 268-274, 2018

[74] Garcia-Esparza, A. T., Cha, D., Ou, Y., Kubota, J., Domen, K., & Takanabe, K.. “Tungsten carbide nanoparticles as efficient cocatalysts for photocatalytic overall water splitting”. *ChemSusChem*, *6*(1), 168-181, 2013

[75] Emin, S., de Respinis, M., Fanetti, M., Smith, W., Valant, M., & Dam, B.. “A simple route for preparation of textured WO_3 thin films from colloidal W nanoparticles and their photoelectrochemical water splitting properties”. *Applied Catalysis B: Environmental*, *166*, 406-412, 2015

[76] What is Spin Coating. (n.d). Retrieved February 28, 2018, from http://www.spincoater.com/what-is-spin-coating.php

[77] Kimmel, Y. C.. Synthesis, characterization, and design of precious metal electrocatalysts supported on transition metal carbides. Unpublished doctoral dissertation, University of Delaware, 2014

[78] X-Ray Principle. (n.d). Retrieved February 28, 2018, from http://www.veqter.co.uk/residual-stress-measurement/x-ray-diffraction

[79] Basic principle of Transmission Electron Microscopy. (n.d). Retrieved February 28, 2018, from http://www.hk-phy.org/atomic_world/tem/tem02_e.html

[80] Principle of Differential Scanning Calorimetry (DSC). (n.d). Retrieved February 28, 2018, from https://www.hitachihightech.com/global/products/science/tech/ana/thermal/descriptions/dsc.html

[81] Differential Scanning Calorimetry (DSC) theory.(n.d).Retrieved February 28, 2018, from http://particle.dk/methods-analytical-laboratory/dsc-differential-scanning-calorimetry-2/dsc-theory/

[82] DSC- Differential Scanning Calorimetry. (n.d). Retrieved February 28, 2018, from http://instrument-specialists.com/thermal-analysisapplications/differential-scanning-calorimetry-dsc/

[83] Ostermayr C. Electrocatalytic activity of platinum on extended gold surfaces and defined gold-nanostructure arrays for the hydrogen reactions. Unpublished doctoral dissertation. Technische Universität München, 2015

[84] X-Ray Photoelectron Spectroscopy. (n.d). Retrieved February 28, 2018, from http://www.npl.co.uk/science-technology/surface-and-nanoanalysis/surface-and-nanoanalysis-basics/introduction-to-xps-x-ray-photoelectron-spectroscopy

[85] Quanta and Wave-Particle Duality. (n.d). Retrieved February 28, 2018, from http://www.physicsoftheuniverse.com/topics_quantum_quanta.html

[86] Potentiostat Fundamentals. (n.d). Retrieved February 28, 2018, from https://www.gamry.com/application-notes/instrumentation/potentiostat-fundamentals/

[87] Basic overview of the working principle of a potentiostat/galvanostat (PGSTAT)–Electrochemical cell setup. (n.d). Retrieved February 28, 2018, from http://www.ecochemie.nl/download/Applicationnotes/Autolab_Application_Note_EC08.pdf

[88] Nahir, T. M., Clark, R. A., & Bowden, E. F.. Linear-sweep voltammetry of irreversible electron transfer in surface-confined species using the Marcus theory. *Analytical Chemistry*, *66*(15), 2595-2598, 1994

[89] Linear Sweep Voltammetry. (n.d). Retrieved February 28, 2018, from https://www.ceb.cam.ac.uk/research/groups/rg-eme/teaching-notes/linear-sweep-and-cyclic-voltametry-the-principles

[90] Electrochemical Impedance Spectroscopy (EIS): A Powerful and CostEffective Tool for Fuel Cell Diagnostics. (n.d). Retrieved February 28, 2018, from http://www.scribner.com/files/tech-papers/Scribner%20Associates%20%20El

ectrochemical%20Impedance%20Spectroscopy%20for%20Fuel%20Cell%20Research.pdf

[91] Electrical Impedance. (n.d). Retrieved February 28, 2018, from http://bmia.bmt.tue.nl/people/BRomeny/Courses/8C120/pdf/ElectricalImpedance.pdf

[92] Emin, S., Altinkaya, C., Semerci, A., Okuyucu, H., Yildiz, A., & Stefanov, P. . Tungsten carbide electrocatalysts prepared from metallic tungsten nanoparticles for efficient hydrogen evolution. *Applied Catalysis B: Environmental*, 236: 147-153, 2018

[93] Hillier, S.. Accurate quantitative analysis of clay and other minerals in sandstones by XRD: comparison of a Rietveld and a reference intensity ratio (RIR) method and the importance of sample preparation. *Clay Minerals*, *35*(1), 291-302, 2000

[94] Koc, R., & Kodambaka, S. K.. "Tungsten carbide (WC) synthesis from novel precursors". *Journal of the European Ceramic Society*, *20*(11), 1859-1869, 2000

[95] Moitra, A., Kim, S., Houze, J., Jelinek, B., Kim, S. G., Park, S. J., German, R. M. & Horstemeyer, M. F. "Melting tungsten nanoparticles: a molecular dynamics study". *Journal of Physics D: Applied Physics*, *41*(18), 185406, 2008

[96] Xu, Y. T., Xiao, X., Ye, Z. M., Zhao, S., Shen, R., He, C. T., et al. Cage-confinement pyrolysis route to ultrasmall tungsten carbide nanoparticles for efficient electrocatalytic hydrogen evolution. *Journal of the American Chemical Society*, *139*(15), 5285-5288, 2017

[97] Hu, Y., Jia, G., Ma, S., Hu, J., Zhu, P., Cui, T., et al. "Hydrogen Evolution Reaction of γ-$Mo_{0.5}W_{0.5}$ C Achieved by High Pressure High Temperature Synthesis". *Catalysts*, *6*(12), 208, 2016.

[98] Shao, Y., Liu, J., Wang, Y., & Lin, Y.. Novel catalyst support materials for PEM fuel cells: current status and future prospects. *Journal of Materials Chemistry*, *19*(1), 46-59, 2009

[99] Wang, X. L., Tang, Y. J., Huang, W., Liu, C. H., Dong, L. Z., Li, S. L., et al. "Efficient electrocatalyst for the hydrogen evolution reaction derived from polyoxotungstate/polypyrrole/graphene". *ChemSusChem*, *10*(11), 2402-2407, 2017

[100] Meng, F., Hu, E., Zhang, L., Sasaki, K., Muckerman, J. T., & Fujita, E.. "Biomass-derived high-performance tungsten-based electrocatalysts on graphene for hydrogen evolution". *Journal of Materials Chemistry A*, *3*(36), 18572-18577, 2015

[101] Chen, W. F., Schneider, J. M., Sasaki, K., Wang, C. H., Schneider, J., Iyer, et al. "Tungsten carbide–nitride on graphene nanoplatelets as a durable hydrogen evolution electrocatalyst". *ChemSusChem*, *7*(9), 2414-2418, 2014

[102] Zeng, M., Chen, Y., Li, J., Xue, H., Mendes, R. G., Liu, J., et al. "2D WC single crystal embedded in graphene for enhancing hydrogen evolution reaction". *Nano Energy*, *33*, 356-362, 2017

[103] Xiao, P., Ge, X., Wang, H., Liu, Z., Fisher, A., & Wang, X.. "Novel molybdenum carbide–tungsten carbide composite nanowires and their electrochemical activation for efficient and stable hydrogen evolution". *Advanced Functional Materials*, *25*(10), 1520-1526, 2015

[104] Fan, X., Zhou, H., & Guo, X.. "WC nanocrystals grown on vertically aligned carbon nanotubes: an efficient and stable electrocatalyst for hydrogen evolution reaction". *ACS nano*, *9*(5), 5125-5134, 2015

[105] Ham, D. J., Ganesan, R., & Lee, J. S.. " Tungsten carbide microsphere as an electrode for cathodic hydrogen evolution from water". *International Journal of hydrogen energy*, *33*(23), 6865-6872.2008

[106] Ko, Y. J., Cho, J. M., Kim, I., Jeong, D. S., Lee, K. S., Park, et al. “Tungsten carbide nanowalls as electrocatalyst for hydrogen evolution reaction: New approach to durability issue”. *Applied Catalysis B: Environmental*, *203*, 684-691, 2017

[107] Liu, Y., Li, G. D., Yuan, L., Ge, L., Ding, H., Wang, D.,et al. “Carbon-protected bimetallic carbide nanoparticles for a highly efficient alkaline hydrogen evolution reaction”. *Nanoscale*, *7(7)*, 3130-3136, 2015

[108] Hunt, S. T., Nimmanwudipong, T., & Román-Leshkov, Y.. “Engineering Non-sintered, Metal-Terminated Tungsten Carbide Nanoparticles for Catalysis”. *Angewandte Chemie International Edition*, *53*(20), 5131-5136, 2014

[109] Chen, Z. Y., Duan, L. F., Sheng, T., Lin, X., Chen, Y. F., Chu, Y. Q., et al. “Dodecahedral W@ WC composite as efficient catalyst for hydrogen evolution and Nitrobenzene reduction reactions”. *ACS applied materials & interfaces*, *9*(24), 20594-20602, 2017

[110] Lin, J. F., Pitkänen, O., Mäklin, J., Puskas, R., Kukovecz, A., Dombovari, et al. “Synthesis of tungsten carbide and tungsten disulfide on vertically aligned multi-walled carbon nanotube forests and their application as non-Pt electrocatalysts for the hydrogen evolution reaction”. *Journal of Materials Chemistry A*, *3*(28), 14609-14616.2015

[111] NikolicaIvan, V. M., Nemanj, M. P., Gavrilov, M., Pašti, I. A., Saponjic, A. B., Vulic, P. et al. “On the tungsten carbide synthesis for PEM fuel cell application–Problems, challenges and advantages”. *International journal of hydrogen energy*, *39*(21), 11175-11185.2014

[112] Ma, C., Sheng, J., Brandon, N., Zhang, C., & Li, G. "Preparation of tungsten carbide-supported nano platinum catalyst and its electrocatalytic activity for hydrogen evolution." *International Journal of Hydrogen Energy*, 32(14) 2824-2829. 2007.

[113] Shang, P., Zhang, J., Tang, W., Xu, Q., & Guo, S.. 2D thin nanoflakes assembled on mesoporous carbon nanorods for enhancing electrocatalysis and for improving asymmetric supercapacitors. *Advanced Functional Materials*, *26*(43), 7766-7774, 2016

CURRICULUM VITAE



PERSONAL INFORMATION

Name Surname : Ali SEMERCİ

Date of Birth : 21.07.1987

E-mail : ali.semerci8@hotmail.com

EDUCATION

Bachelor: Sakarya University/ ADAPAZARI (2008-2012) (3.21/4.00)

Master Degree: Ankara Yıldırım Beyazıt University (2016- 2018)

WORK EXPERIENCE

Research Assist.: Ankara Yıldırım Beyazıt University / (2016- contunied)

Türk-Alman University / (2016 March-October)

TOPICS OF INTEREST

- Renewable Energy
- Hydrogen Production
- Solar Cell

PUBLISHED WORKS (SCI)

1. Emin, S., Altinkaya, C., **Semerci, A.,** Okuyucu, H., Yildiz, A., & Stefanov, P. Tungsten carbide electrocatalysts prepared from metallic tungsten nanoparticles for efficient hydrogen evolution. *Applied Catalysis B: Environmental*, 236: 147-153, 2018

CONFERENCE PROCEEDINGS

1. Emin, S., Altinkaya, C., **Semerci, A**., Okuyucu, H., Yildiz, A.. Tungsten Carbide Thin Films for Electrochemical Water Splitting. *International Conference on Functional Nanomaterials and Nanodevices/Budapest, ISBN:* 978-954-2987-31-4, *128, 2017*